NOAA Technical Memorandum ERL PMEL-62

THEORETICAL AND OBSERVED PROFILES OF TIDAL CURRENTS AT TWO SITES ON THE SOUTHEASTERN BERING SEA SHELF

Harold O. Mofjeld
James D. Schumacher
David J. Pashinski

Pacific Marine Environmental Laboratory
Seattle, Washington
October 1984

UNITED STATES
DEPARTMENT OF COMMERCE

Malcolm Baldrige,
Secretary

NATIONAL OCEANIC AND
ATMOSPHERIC ADMINISTRATION

John V. Byrne,
Administrator

Environmental Research
Laboratories

Vernon E. Derr
Director

NOTICE

Mention of a commercial company or product does not constitute an endorsement by NOAA Environmental Research Laboratories. Use for publicity or advertising purposes of information from this publication concerning proprietary products or the tests of such products is not authorized.

CONTENTS

ABSTRACT

A semi-analytic theory for vertical profiles of tidal currents on the continental shelf is presented in which the vertical eddy viscosity is obtained with a high-resolution, Level II turbulence closure model. Each tidal constituent is assumed to be a free, shallow water wave propagating on an unstratified shelf of constant depth. The eddy viscosity is a time-dependent composite of contributions from the major tidal constituents. The theoretical profiles have been fit to M2 and K1 current harmonic constants observed at two sites on the Southeastern Bering Sea Shelf. At the coastal station BBL1 (56°19'N, 161°33'W; 63 m depth) off the Alaska Peninsula occupied during 15-30 May 1981 in a Kelvin wave regime with rectilinear tidal currents, the fit of M2 and K1 theoretical profiles reproduces the general features of the tidal currents. The thick bottom boundary layers observed at BBL1 require a large apparent bottom roughness (1.0 cm) which may be due to strong surface swell and/or bedforms. The predicted eddy viscosity has a maximum of 400 cm^2/s located at a height of 20 m above the bottom. At the mid-shelf station BBL2 (57°37'N, 167°45'W; 69 m depth) occupied during 28 July - 5 August 1982 in a Sverdrup wave regime with rotatory tidal currents, the fit to the thin boundary layers observed for M2 and K1 reveals a small apparent bottom roughness (0.001 cm), possibly due to calm weather and/or the lack of bedforms. The theory overestimates slightly the width of the M2 ellipses but predicts the K1 width and the perpendicular orientation of the M2 and K1 ellipses. The predicted eddy viscosity at BBL2 has a maximum of 250 cm^2/s at a height of 25 m. The theory provides estimates of residual tidal currents under very restrictive assumptions. For the coastal Kelvin waves propagating along the Alaska Peninsula, the residual tidal current (sum of O1, K1, N2 and M2) is due almost entirely to Stokes drift and produces a transport of $\sim 2(10)^5 m^3/s$ toward Bristol Bay. For the Sverdrup waves in the mid-shelf regime, the magnitudes of the theoretical residual currents are a factor of 1/20 smaller than the coastal currents although bottom topography (not in the theory) can generate much stronger residual currents.

1. INTRODUCTION

This memorandum presents a theory for the vertical profiles of tidal currents and a comparison of the theory with observations at two sites on the Southeastern Bering Sea Shelf. The tidal currents are assumed in the theory to vary with height above the bottom because of eddy viscosity. The eddy viscosity is obtained through a second-order turbulence closure model. Effects of stratification, ice cover and bottom slope are neglected. The theory also gives estimates of residual tidal currents subject to very restrictive assumptions.

Following a classical approach to the analysis of tidal motions on the shelf (Sverdrup, 1927; Thorade, 1928; Fjeldstad, 1929; [see Defant, 1961, for a summary of this work]; Mofjeld, 1980), each tidal constituent is assumed to be a free, shallow water wave propagating on a shelf of constant depth. The theory can be easily extended to a combination of waves. The tidal currents of the constituent are decomposed into clockwise and counter-clockwise-rotating components which satisfy viscous vertical structure equations. The eddy viscosity is a time-independent composite of contributions from the major tidal constituents, similar to the method of Smith and Long (1976). One advantage of this approach is that each tidal constituent is governed by a linear set of equations.

The eddy viscosity is computed with a Level II second-order turbulence closure model (Mellor and Yamada, 1974, 1982; Mofjeld and Lavelle, 1984; Overland, Mofjeld and Pease, 1984). In the model, the viscosity is proportional to the product of the turbulence intensity and a mixing length. The turbulence intensity (square root of twice the turbulence kinetic energy) is determined by a balance in the water column between local shear production and dissipation. The mixing length near the bottom increases linearly with height and goes smoothly to an asymptotic value well-above the bottom. The model is iterated until the friction velocity (square root of the bottom stress magnitude) has settled down within 10^{-3} cm/s.

To calibrate and test the theory, two sites on the Southeastern Bering Sea Shelf (Figure 1) were occupied with dense arrays of current meters near the bottom. Tidal models (Sündermann, 1977; Liu and Leenderste, 1978, 1979, 1982, 1984; Isaji, Spaulding and Reed, 1984) and observations (Pearson, Mofjeld and Tripp, 1981) show that the tides along the Alaska Peninsula are Kelvin waves incident from the deep Aleutian Basin. One of the sites BBL

(Figure 1) was occupied during 15-30 May 1981 in the Kelvin wave regime where the tidal currents are relatively strong and rectilinear. The second site BBL2 was located in the mid-shelf regime where the tidal currents have smaller speeds and broad current ellipses. It was occupied during 28 July - 5 August 1982. As with the outer reaches of the Northeastern Bering Sea Shelf (Mofjeld, 1984), the tidal currents near BBL2 closely resemble Sverdrup waves incident from the Aleutian Basin. The analysis was carried out for the four major tidal constituents (O1, K1, N2 and M2) of the Bering Sea (Pearson, *et al.*, 1981). The comparison of the theoretical and observed profiles help to show the power and limitations of this simple theory.

Theoretical estimates for the residual tidal currents have been obtained for Kelvin and Sverdrup waves tuned to the observations using the approach of Dvoryaninov and Prusov (1978). Stokes drifts, Eulerian and Lagrangian currents computed for each type of wave give useful insight into the dynamics of these currents although it must be recognized that a tidal model of the entire Eastern Bering Sea Shelf is required to give reliable estimates of the actual residual currents. Such estimates have been made by Sündermann (1977), Liu and Leenderste (1978, 1979, 1982 and 1984), and Isaji *et al.* (1984). A first guess at the effects of local bottom slope on the character of the residual currents is also made in this memorandum.

2. THEORETICAL FORMULATION

a. Tidal Currents

The theoretical profiles of tidal currents and locally-generated residual tidal currents are obtained by solving a set of differential equations. The currents are described in terms of their east u and north v components. Under the assumptions that the tidal motion are driven by horizontal pressure gradients and that these gradients are independent of depth (long waves unaffected by stratification), the tidal pressure is described entirely by the sea surface displacement η_s. As discussed by Mofjeld (1980), the tides and tidal currents satisfy the linearized equations of motion

$$\frac{\partial u}{\partial t} - fv = -g \frac{\partial \eta_s}{\partial x} + \frac{\partial}{\partial z}\left[A \frac{\partial u}{\partial z}\right] \tag{1}$$

$$\frac{\partial v}{\partial t} + fu = -g \frac{\partial \eta_s}{\partial y} + \frac{\partial}{\partial z}\left[A \frac{\partial v}{\partial z}\right] \tag{2}$$

$$\frac{\partial \eta_s}{\partial t} + \int_{z_o}^{H} \frac{\partial u}{\partial x} + \frac{\partial v}{\partial y}\, dz = 0 \tag{3}$$

with time t, east-, north- and vertical coordinates x, y, z, Coriolis parameter f, acceleration of gravity g, eddy viscosity A, bottom roughness length z_o and mean depth H.

At the bottom, friction causes the tidal currents to be zero

$$u, v = 0 \quad \text{at} \quad z = z_o \tag{4}$$

At the surface, the stress is assumed to be zero which is equivalent to requiring that the vertical gradients of velocity be zero

$$\frac{\partial u}{\partial z}, \frac{\partial v}{\partial z} = 0 \quad \text{at } z = H \tag{5}$$

This surface condition precludes the presence of floating ice of sufficient rigidity to produce major drag on the water. The present study focuses on the bottom boundary layers during the summer when the bottom boundary layer observations were taken. Pearson, Mofjeld and Tripp (1981) observed tidal currents on the eastern Bering Sea Shelf which apparently change significantly between ice-free and ice-covered conditions. However, the apparent change may be due to a suppression of rotor-pumping by ice rather than a dynamic process at work in the water as discussed by Mofjeld (1984). The influence of ice on tidal currents is beyond the scope of the present work.

The eddy viscosity is given by

$$A = \ell^2 \left[\left(\frac{\partial u}{\partial z} \right)^2 + \left(\frac{\partial v}{\partial z} \right)^2 \right]^{1/2} \tag{6}$$

where the mixing length ℓ is taken the form

$$\ell = kz/(1 + kz/\ell_o) \tag{7}$$

which is recommended for boundary layers by Blackadar (1962) and Mellor and Yamada (1974, 1982). Well-above the bottom, the mixing length ℓ reaches its asympotic value ℓ_o which is assumed to be determined by the vertical scale of the turbulent intensity q

$$\ell_o = \gamma \int_{z_o}^{H} zq\,dz / \int_{z_o}^{H} q\,dz \tag{8}$$

As found by Mofjeld and Lavelle (1984), the appropriate value of γ is 0.2. This value was arrived at through matching this Level II model to the similarity theory of Businger and Arya (1974) for the steady Ekman layer as well as through a fit of the model to observed M2 tidal currents in Admiralty Inlet, Washington.

The turbulent intensity of (square root of twice the turbulent energy density) is given by a local balance between shear production and viscous dissipation

$$0 = - A \frac{\partial u}{\partial z} \frac{\partial u}{\partial z} - -A \frac{\partial v}{\partial z} \frac{\partial v}{\partial z} - \frac{q^3}{c\ell} \qquad (9)$$

As shown by Mofjeld and Lavelle (1984), the velocity components u, v and eddy viscosity A are independent of the dissipation constant c while the turbulent intensity q has a weak $c^{1/3}$ dependence. In the calculations, c was set equal to 12.0. Because we are considering the bottom boundary layer away from sources of stratified water such as the shelfbreak or the pycnocline, stratification is neglected in equation (9).

In the profile model of tidal currents, it is assumed that the eddy viscosity is independent of time. This is because the observations to which the model will be compared are the major harmonic constants which are a part of the total tidal signal that is affected by the time-average of eddy viscosity. The time-dependence in the eddy viscosity gives rise to higher frequency tidal constituents not resolved in the observations. A discussion of how the time-dependence of the eddy viscosity affects rectilinear tidal currents (Kelvin wave-like) is given by Lavelle and Mofjeld (1983). Rotary tidal constituents with broad ellipses such as those in the mid-shelf region of the Eastern Bering Sea Shelf show little change in speed over the tidal cycle and the eddy viscosity due to a given tidal constituent is relatively independent of time.

In the model, we allow the four largest tidal constituents O1, K1, N2 and M2 to contribute to the eddy viscosity. Because of the short length and noise content of the bottom boundary layer observations, each tidal band has to be considered as a unit (1 complex weight per band) in the response tidal

analyses. This fixes the relative amplitudes and phases in a given band. Hence the comparison of the Level II model and observations can be made with the largest constituents in the principal bands: M2 for the semidiurnal band and K1 for the diurnal band.

Following the standard procedure developed by Sverdrup (1927) and discussed by Mofjeld (1980) components of a given tidal constituent may be written as a sum of clockwise q and counterclockwise r rotating components

$$u = (q + r)/2 \quad , \quad v = (q - r)/2i \tag{10}$$

The horizontal equation of motion (1) and (2) for the rotating components (Mofjeld, 1980) are most conveniently written in terms of velocity defects q', r':

$$q = Q(1 - q') \quad , \quad r = R(1 - r') \tag{11}$$

$$\frac{\partial}{\partial z}\left[A \frac{\partial q'}{\partial z}\right] + i(\omega - f)q' = 0, \quad \frac{\partial}{\partial z}\left[A \frac{\partial r'}{\partial z}\right] + i(\omega + f)r' = 0 \tag{12}$$

with

$$q', r' = 1 \text{ at } z = z_o \quad ; \quad \frac{\partial q'}{\partial z} \quad , \quad \frac{\partial r'}{\partial z} = 0 \quad \text{at } z = H \tag{13}$$

where the amplitudes of the rotating components q, r are given by depth-independent amplitudes Q,R that satisfy the relations derived from the momentum equations (1) and (2)

$$Q = -ig\left[\frac{\partial \eta_s}{\partial x} + i \frac{\partial \eta_s}{\partial y}\right]/(\omega - f) \quad , \quad R = -ig\left[\frac{\partial \eta_s}{\partial x} - i \frac{\partial \eta_s}{\partial y}\right]/(\omega + f) \tag{14}$$

We shall assume that the tides and tidal currents at the two selected sites are simple tidal waves. As we shall see, these assumptions work well for the tidal currents at these two bottom boundary layer stations.

For a planar wave

$$\eta_s = \eta_o \exp[i(k_x x + k_y y - \omega t)] \tag{15}$$

the dispersion relation for these waves (Mofjeld, 1980) relating the wavenumber components to the angular frequency ω is obtained by substituting (11)-(14) into the equation of continuity (3)

$$k_x^2 + k_y^2 = (\omega^2 - f^2)/gH_e \tag{16}$$

The equivalent depth H_e is given by

$$H_e = H - z_o + \frac{i}{2\omega} \left\{ \frac{\omega+f}{\omega-f} \left[A \frac{\partial q'}{\partial z} \right] + \frac{\omega-f}{\omega+f} \left[A \frac{\partial r'}{\partial z} \right] \right\}_{z=z_o} \tag{17}$$

One more condition is needed between the wavenumber components. For the Sverdrup wave, we rotate the coordinate system so that the negative y-axis is parallel to the direction of propagation. The mid-shelf station BBL2 is far enough from lateral boundaries that the wave can be considered independent of the x-direction.

$$k_x = 0 \text{ for the Sverdrup waves} \tag{18}$$

As we shall see later, the observed relationship between the tides and tidal currents in the mid-shelf region indicate that the tidal motions there are combinations of incident and reflected Sverdrup waves. In looking at the tidal currents alone, we can use the same condition (18) on k_x. The effect of having a super-position of Sverdrup waves is to have partial cancellation of the residual currents.

The coastal Kelvin wave has a component of velocity transport in the bottom boundary layer in the direction perpendicular to the coast. This

transport component must be balanced (Mofjeld, 1980) by a compensating transport in the rest of the water column because there can be no net transport through the coast

$$\int_{z_o}^{H} u \, dz = 0 \tag{19}$$

where the Kelvin wave is assumed to propagating in the negative y-direction. This condition produces an equation between the wavenumber components

$$H_e k_x + i \Gamma k_y = 0 \quad \text{for the Kelvin waves} \tag{20}$$

where

$$\Gamma = H - z_o + \frac{i}{2\omega} \left\{ \frac{\omega+f}{\omega-f} \left[A \frac{\partial q'}{\partial z} \right] - \frac{\omega-f}{\omega+f} \left[A \frac{\partial r'}{\partial z} \right] \right\}_{z=z_o} \tag{21}$$

At the bottom, the magnitude of the stress exerted by the water on the bottom is assumed to be of the form

$$u_*^2 = A \left[\left(\frac{\partial u}{\partial z} \right)^2 + \left(\frac{\partial v}{\partial z} \right)^2 \right]^{\frac{1}{2}} \quad \text{at } z=z_o \tag{22}$$

where u_* is a time-independent friction velocity defined as the square root of the kinematic stress. In the expression (22), the shears $\frac{\partial u}{\partial z}$ and $\frac{\partial v}{\partial z}$ are sums over four tidal constituents O1, K1, N2 and M2. This sum produces the upper limit on u_* based on these four constituents since cancelling is not allowed between the constituents and the contribution of a given constituent is $2^{\frac{1}{2}}$ times the time-average for that constituent. An adjustment of the bottom roughness z_o can be used to compensate for the factor $2^{\frac{1}{2}}$. This overestimate for the four constituents tends to compensate for the contributions to u_* that are not made by neglected constituents. The details of cancellation between constituents is beyond this analysis.

To compute the residual currents, it is necessary to have profiles of the vertical velocity and displacement. The vertical displacement η at a height z is given by

$$\eta = \eta_s \ (z_e/H_e) \tag{23}$$

where

$$z_e = (z-z_o) + \frac{i}{2\omega}\left\{ \frac{\omega+f}{\omega-f}\left[A\frac{\partial q'}{\partial z}\right] + \frac{\omega-f}{\omega+f}\left[A\frac{\partial r'}{\partial z}\right]\right\}_{z=z_o}^{z} \tag{24}$$

for a tidal constituent with angular frequency ω. The vertical velocity w for the same constituent is given by

$$w = -i\omega\eta \tag{25}$$

The equations (1)-(25) are solved numerically using a fourth-order Runge-Kutta scheme. The integration is performed downward from the surface and renormalized to match the boundary conditions at the bottom. A variable grid is used to provide high resolution near the bottom. The value of the height z at each grid point are given by the implicit equation

$$s = az + b\ \log(z) + c \tag{26}$$

where s is the index of the grid point and the constants a, b, c are such that half the grid points lie between z=1m and the bottom $z=z_o$; s=1 at $z=z_o$ and s=2001 at z=H. The grid has a total of 1000 intervals divided into two subintervals each. The formula (26) is used when s is an odd number. For s even, z is halfway between adjacent values of z as required by the Runge-Kutta scheme.

Using an initial profile of viscosity based on a linear-times-exponential Businger-Arya form, profiles of velocity and an initial estimate of the friction velocity u_* are obtained. A new profile of viscosity is then computed and hence a new value for u_*. The procedure is continued until the values of u_* from successive interations differ by less than $1.0(10)^{-3}$cm/s. Instabilities in the interation scheme are avoided by setting the viscosity profile equal to the mean of the two previous profiles.

b. Residual Currents

The residual tidal currents are assumed here to be generated locally over a horizontal bottom (residual tidal currents generated over a sloping bottom are discussed briefly in the Results of Modeling Section). There are three kinds of residual currents: Eulerian currents, Stokes drifts and Lagrangian currents. Eulerian currents are generated by divergences in the tidal Reynolds stresses. These are the residual currents that can be directly sensed by current meters as mean currents. The Stokes drifts arise from spatial variations in the tidal currents that cause a given water parcel to end up at a different location at the end of a tidal cycle than where it began. The Lagrangian currents are the sums of the Eulerian currents and the Stokes drift. They represent the total mass transport induced by the tides and tidal currents.

We assume that the Eulerian currents components u_E, v_E satisfy the equations

$$-fv_E = -\sum_n \left[\overline{u_n \frac{\partial u}{\partial x} n} + \overline{v_n \frac{\partial u}{\partial z} n} + \overline{w_n \frac{\partial u}{\partial z} n} \right] + \frac{\partial}{\partial z} \left[A \frac{\partial u}{\partial z} E \right] \qquad (27)$$

$$fu_E = -\sum_n \left[\overline{u_n \frac{\partial v}{\partial x} n} + \overline{v_n \frac{\partial v}{\partial z} n} + \overline{w_n \frac{\partial v}{\partial z} n} \right] + \frac{\partial}{\partial z} \left[A \frac{\partial v}{\partial z} E \right] \qquad (28)$$

where the summation is over the four tidal constituents O1, K1, N2 and M2 and the overbars denote time-averages. In (27) and (28), each tidal constituent contributes individually to the total Eulerian current without cross-modulation with the other constituents. We are therefore excluding low-frequency oscillations of fortnightly (two-week) and longer periods generated by the non-linear interaction of the tidal constituents. The viscosity is that computed by the profile model for the tidal constituents.

The Eulerian currents are subject to the same boundary conditions as the tidal currents: zero velocity at the bottom

$$u_E, v_E = 0 \quad \text{at} \quad z = z_o \qquad (29)$$

and zero shear at the surface

$$\frac{\partial u}{\partial z} E , \frac{\partial v}{\partial z} E = 0 \quad \text{at } z = H \qquad (30)$$

We write the total Stokes drift as a sum of contributions from the individual constituents

$$u_S = \sum_n \left[\overline{\Delta X_n \frac{\partial u}{\partial x} n} + \overline{\Delta Y_n \frac{\partial u}{\partial y} n} + \overline{\eta_n \frac{\partial u}{\partial z} n} \right] \qquad (31)$$

$$v_S = \sum_n \left[\overline{\Delta X_n \frac{\partial v}{\partial x} n} + \overline{\Delta Y_n \frac{\partial v}{\partial y} n} + \overline{\eta_n \frac{\partial v}{\partial z} n} \right] \qquad (32)$$

where the horizontal displacements ΔX_n and ΔY_n are time-integrals of the horizontal velocity components

$$\Delta X_n = i u_n / \omega_n \quad , \quad \Delta Y_n = i v_n / \omega_n \qquad (33)$$

A derivation of the formulas for the Stokes drift is given by Longuet-Higgins (1969).

The total mass transport is given by the sum of the Eulerian currents and the Stokes drifts. These Lagrangian currents are written simply as

$$u_L = u_E + u_S \quad , \quad v_L = v_E + v_S \tag{34}$$

3. OBSERVATIONS OF TIDAL CURRENT PROFILES

Detailed profiles of tidal currents were measured at two stations (Fig. 1) on the southeastern Bering Sea Shelf. Station BBL1 (56°19'N, 161°33'W; 63m depth) was deployed about 50km northwest of Port Moller. The tidal currents (Fig. 2) in this coastal region are relatively strong and flow parallel to the general trend of the adjacent coast. Station BBL2 (57°37'N, 167°45'W; 69m depth) was deployed in the mid-shelf region (Fig. 1) about 130 km northeast of the Pribilof Island where the tidal currents (Fig. 2) are characterized by broad tidal ellipses.

Two moorings were deployed at each station. At BBL1 Neil-Brown acoustic current meters were placed on one mooring at heights of 14, 35, 44, 49 and 59m above the bottom. On a shorter mooring were Aanderaa current meters at heights of 1, 3 and 5m. At BBL2 Neil-Brown acoustic current meters were used throughout. Meters were placed at heights of 5, 15 and 30m on one mooring and 1, 3, 5m on the other.

The two stations were occupied during different years. BBL1 yielded time series of currents over the period 15-30 May 1981 while the current records at BBL2 span the period 28 July - 5 August 1982. A mooring was deployed at BBL2 during 1981 but it was lost during the recovery operation.

The current records were analyzed for tidal currents using the response method. This method finds the relative amplitudes and phases of the tidal constituents with respect to a reference series. The relative quantities are combined with the harmonic constants for the reference series to produce harmonic constants for the observed series. The analyses are performed on the east and north components of the currents and the resulting harmonic

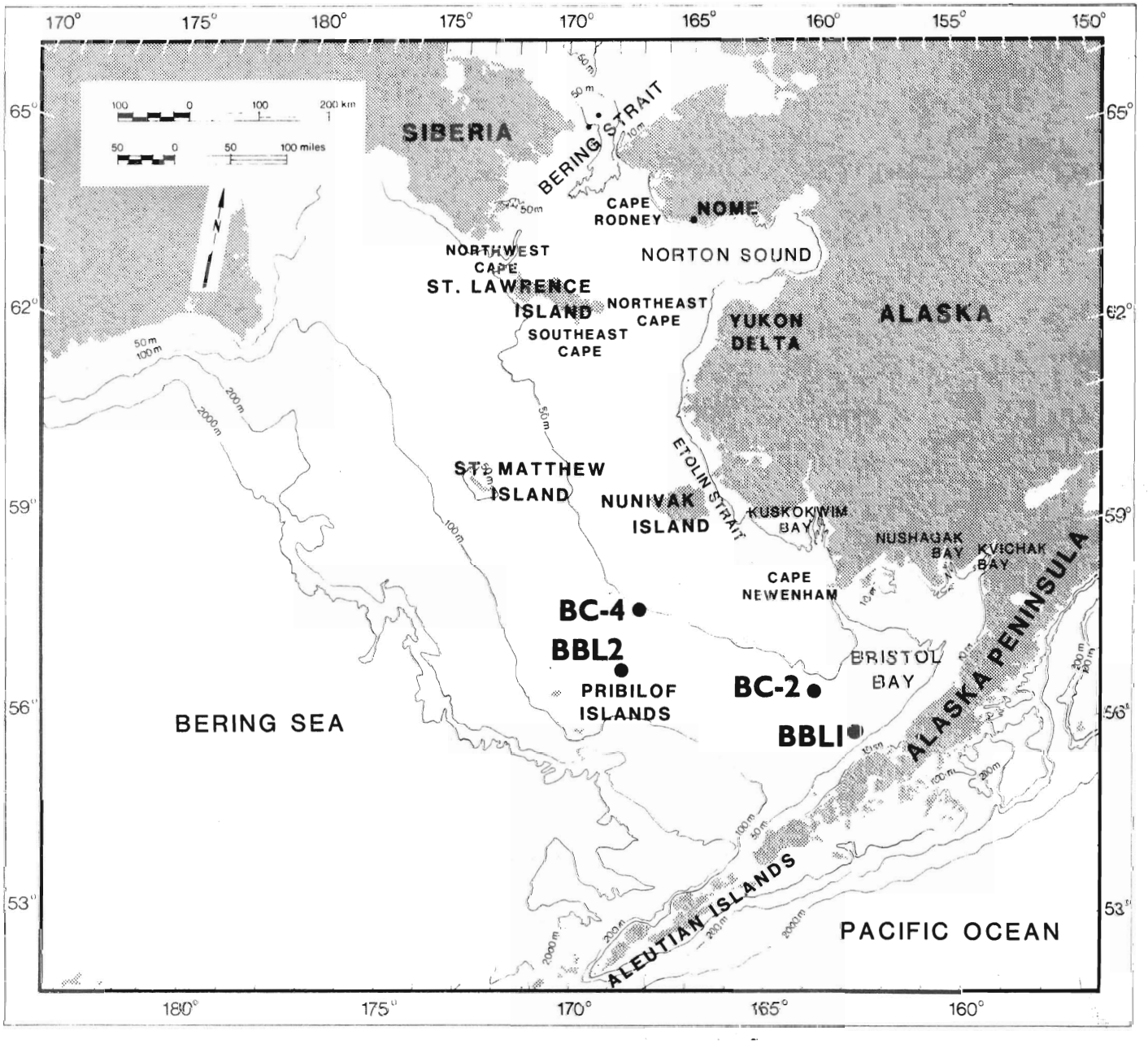

Figure 1. Chart of the Eastern Bering Sea Shelf showing the locations of the bottom boundary layer stations BBL1 and BBL2 and their corresponding reference stations BC-2 and BC-4 for response tidal analyses.

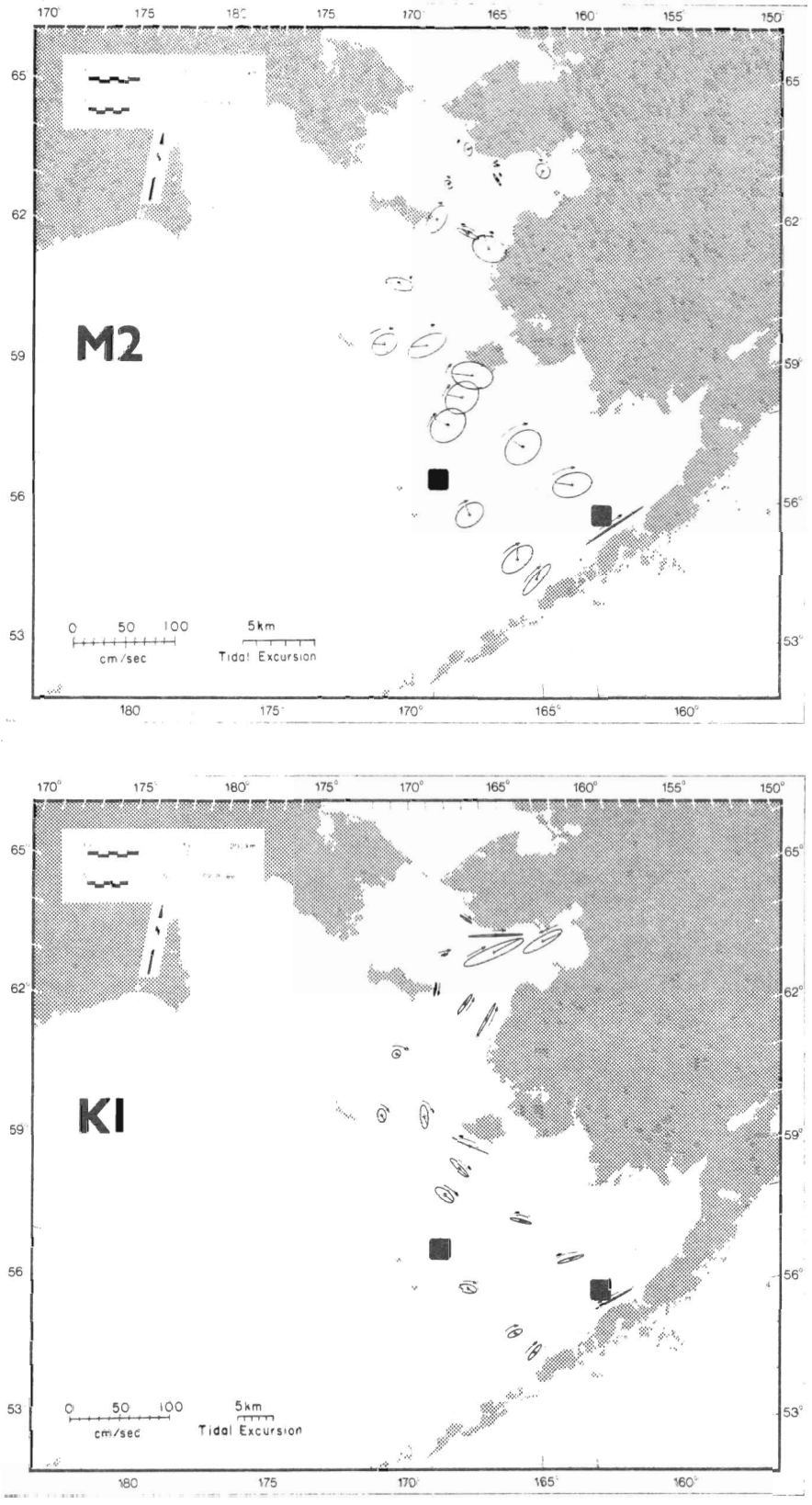

Figure 2. Observed M2 and K1 tidal ellipses on the Eastern Bering Sea Shelf. Arrows outside the ellipses show the sense of rotation of the velocity vectors with time. Lines from the centers of the ellipses show the velocity vector at the time of Greenwich transit for that tidal constituent. From Pearson, Mofjeld and Tripp (1981).

constants are then converted into the parameters of the tidal ellipses. Because the current records are short, one complex weight per tidal band was used in the correlations between the observed and reference series. This choice for the number of complex weights is equivalent to the assumption that the internal relationships of the tidal constituents within a given tidal band are the same in the observed and reference series. It is therefore important that the observed and reference series have similar tidal characteristics.

The response method provides an estimate for the accuracy of the harmonic constants of the east and north components. The estimate is obtained by comparing the residual variance (left in each tidal band after analysis) with the predicted variance. If the ratio of residual to predicted variance is small, the analysis has succeeded in explaining a large part of the tidal signal. A large residual variance indicates that much tidal variance remains after analysis and that the estimated harmonic constants may not accurately represent those at the station. Large residual variances may be caused by a number of problems including a small tidal signal, a poor choice of reference series, an incorrect time base for the reference or observed series and faulty current sensors.

The results of the tidal analysis on the current records from BBL1 are given in Tables 1-6. The reference series was the predicted tide at BC-2 (57°04'N, 163°22'W) based on the tidal harmonic constants shown in Table 1. The current harmonic constants of the major tidal constituents O1, K1, N2 and M2 for BBL1 are shown in Table 2. Ordinarily S2 would be included in such a list but it is a minor constituent in the Bering Sea (Pearson, Mofjeld and Tripp, 1981). The tidal analyses were performed over the full length (378 hours) of each acoustic current meter record. Table 3 shows that the

Table 1. Reference tidal harmonic constants from BC-2 (57°04'N, 163°22'W) used in the response analyses of the coastal station BBL1.

Constit.	Period (hours)	Amplitude (cm)	Greenwich Phase Lag (°G)	Amplitude Ratio	Relative Phase Lag (°)
Q1	26.87	3.7	351	0.131	-22
O1	25.82	19.0	358	0.671	-15
M1	24.84	1.1	6	0.039	-7
P1	24.07	9.3	11	0.329	-2
K1	23.93	28.3	13	1.000	0
J1	23.10	1.7	19	0.060	6
OO1	22.31	1.0	25	0.035	12
2N2	12.91	2.0	47	0.044	-110
μ2	12.87	1.8	47	0.040	-110
N2	12.66	14.7	102	0.325	-55
ν2	12.63	2.8	109	0.062	-48
M2	12.42	45.2	157	1.000	0
L2	12.19	0.6	153	0.013	-4
(T2)[1]	(12.02)	(0.1)	(350)	(0.002)	(193)
S2	12.00	0.5	343	0.011	186
K2	11.97	0.1	343	0.002	186

[1] not used in response analyses

Table 2. Current harmonic constants for O1, K1, N2, M2 from the acoustic current meter data at the coastal station BBL1 (56°19'N, 161°33'W; 63 m depth) obtained by the response method (1 complex weight per tidal band; 378 hour series length) with predicted tides at BC-2 (Table 1) as the reference.

Constit.	Height (m)	Amplitudes Major (cm/s)	Amplitudes Minor (cm/s)	Greenwich Phase Lag[1] (°G)	Orientation of Major Axis (°True)	Sense of Rotation[2]
O1	59	15.90	0.39	290.3	77.3	C
	49	15.03	0.18	293.5	76.0	CC
	44	13.62	0.12	298.1	71.1	CC
	35	13.37	0.26	300.4	71.9	CC
	14	12.33	1.04	307.7	60.1	CC
K1	59	23.68	0.58	305.3	77.3	C
	49	22.38	0.27	308.5	76.0	CC
	44	20.29	0.18	313.1	71.1	CC
	35	19.92	0.39	315.4	71.9	CC
	14	18.36	1.55	322.7	60.1	CC
N2	59	12.90	0.72	116.9	64.7	C
	49	11.96	0.61	117.8	64.9	C
	44	11.05	0.69	119.4	62.9	C
	35	11.04	0.54	114.5	67.0	C
	14	8.67	1.55	95.0	80.8	CC
M2	59	39.67	2.22	171.9	64.7	C
	49	36.76	1.88	172.8	64.9	C
	44	33.98	2.13	174.4	62.9	C
	35	33.97	1.67	169.5	67.0	C
	14	26.69	4.77	150.0	80.8	CC

[1]Major Axis

[2] C = Clockwise
CC = Counterclockwise

Table 3. Reductions in variance as a result of response tidal analyses applied to the acoustic current meter data at the coastal station BBL1. Small residual variances and reductions near 100% indicate that almost all the variance in a given tidal band is accounted for by the predicted tidal currents resulting from the response method.

Component	Tidal Band	Height (m)	Variance Predicted $(cm/s)^2$	Variance Residual $(cm/s)^2$	Reduction in Variance (%)
East	Diurnal	59	438.34	24.84	94.33
		49	387.40	13.26	96.58
		44	302.74	9.82	96.76
		35	294.42	10.97	96.27
		14	208.32	3.50	98.32
North	Diurnal	59	22.60	5.00	77.88
		49	24.06	2.36	90.19
		44	35.33	3.09	91.25
		35	31.50	2.23	92.92
		14	70.30	3.74	96.68
East	Semi-diurnal	59	385.08	6.37	98.35
		49	331.60	6.26	98.11
		44	273.61	5.13	98.13
		35	292.17	2.96	98.99
		14	207.34	7.40	96.43
North	Semi-diurnal	59	86.89	1.29	98.52
		49	73.45	2.62	96.43
		44	72.91	1.77	97.57
		35	53.50	1.55	97.10
		14	12.09	0.81	93.30

reductions in variance were quite good and the harmonic constants can therefore be expected to represent accurately those at BBL1. The Aanderaa records at BBL1 suffered from speed and time base problems. It was convenient to analyze the Aanderaa records in 3-day segments to isolate these problems. The most reliable harmonic constants were assumed to be those for which there was an excellent reduction in variance although the phase may still be in error due to time base problems earlier in the records. The harmonic constants for the Aanderaa records at BBL1 are given in Table 4 and the reductions in variance in Table 5 and 6.

The results of the analyses for the mid-shelf station BBL2 are given in Table 7-9. The reference series was the predicted tidal current at BC-4 (58°37'N, 168°14'W) based on the harmonic constants for BC-4 in Table 7. The values for the 30m height (Table 8) at BBL2 are in parentheses because of a possible defect in the current record. After recovery it was discovered that the corresponding current meter had lost an acoustic mirror in the current sensor. A comparison of results (Table 8) for the 30m height with the results at other heights reveals significant differences. There were two current meters deployed at the 5m height, one on each mooring. From Table 8 it can be seen that the differences in amplitudes for the two current meters at the 5m height is significantly less than the differences between heights. It appears then that the amplitude profile is well-resolved at BBL2. This is partially true for the phase lags and orientations (Table 8). The orientation at the lm height may have been contaminated by magnetic interference from the steel anchor because both M2 and K1 show the same deviation in direction at the 1 m height relative to the directions measured above.

Table 4. Current harmonic constants for O1, K1, N2, M2 from the near-bottom Aanderaa current meter data at the coastal station BBL1 (56°19'N, 161°33'W; 63 m depth) obtained by the response method (1 complex weight per tidal band) applied to 3-day segments with predicted tides at BC-2 (Table 4) as the reference. The procedure for estimating the harmonic constants of other constituents is the same as that given in Table 2.

Constit.	Height (m)	Segments	Amplitudes Major (cm/s)	Amplitudes Minor (cm/s)	Greenwich Phase Lag (°G)	Orientation of Major Axis (°True)	Sense of Rotation
K1	5	1	16.86	3.49	144.0	238.9	CC
		2	16.76	5.66	146.7	229.8	CC
		3	13.13	3.08	137.9	228.7	CC
		4	15.59	3.27	130.5	227.4	CC
		5	19.41	3.81	138.5	231.1	CC
K1	3	1	15.21	4.60	141.3	237.8	CC
		2	15.30	5.59	145.8	235.2	CC
		3	13.30	3.18	136.4	236.1	CC
		4	15.05	3.22	133.8	232.5	CC
		5	15.74	3.84	111.2	237.3	CC
K1	1	1	13.77	4.20	140.8	237.1	CC
		2	13.51	5.01	119.6	236.0	CC
		3	6.75	2.27	173.3	215.2	CC
		4	11.65	1.45	180.9	228.8	CC
M2	5	1	15.70	3.82	334.4	249.4	CC
		2	21.91	7.34	320.0	258.9	CC
		3	19.34	4.99	322.5	251.3	CC
		4	22.40	6.81	311.8	262.7	CC
		5	25.38	5.57	322.3	253.6	CC
M2	3	1	21.73	7.17	326.3	261.9	CC
		2	20.44	6.94	320.3	263.5	CC
		3	18.58	5.50	323.6	256.5	CC
		4	22.35	7.36	314.1	269.0	CC
		5	16.40	3.96	259.7	255.0	CC
M2	1	1	19.69	6.89	326.5	262.7	CC
		2	14.18	5.22	283.1	260.3	CC
		3	9.05	6.53	166.9	238.6	CC
		4	21.52	6.20	53.7	265.3	CC

Table 5. Reductions in variance for the diurnal band as a result of response analyses applied to 3-day segments of the near-bottom Aanderaa current meter data at the coastal station BBL1.

Component	Tidal Band	Height (m)	Segment	Variance Predicted $(cm/s)^2$	Variance Residual $(cm/s)^2$	Reduction in Variance (%)
East	Diurnal	5	1	41.80	3.59	91.41
			2	117.35	11.15	90.50
			3	111.65	2.36	97.89
			4	129.67	0.31	99.76
			5	76.14	2.62	96.56
North	Diurnal	5	1	17.14	0.35	97.96
			2	96.37	3.78	96.08
			3	87.76	3.69	95.80
			4	103.87	0.17	99.84
			5	36.77	1.78	95.16
East	Diurnal	3	1	29.17	1.34	95.14
			2	112.12	9.51	91.52
			3	137.94	0.44	99.68
			4	136.85	0.44	99.68
			5	56.13	6.17	89.01
North	Diurnal	3	1	15.63	0.36	97.70
			2	69.26	6.34	90.85
			3	68.37	6.03	91.18
			4	81.37	0.04	99.95
			5	19.92	1.10	94.48
East	Diurnal	1	1	23.41	0.91	96.11
			2	92.60	2.35	97.46
			3	22.21	11.85	46.65
			4	83.89	1.50	98.21
North	Diurnal	1	1	13.25	0.39	97.06
			2	53.56	3.65	93.19
			3	35.89	9.50	73.53
			4	56.44	0.29	99.49

Table 6. Reduction in variance for the semidiurnal band as a result of response and analyses applied to 3-day segments of the near-bottom Aanderaa current meter data at the coastal station BBL1.

Component	Tidal Band	Height (m)	Segment	Variance Predicted $(cm/s)^2$	Variance Residual $(cm/s)^2$	Reduction in Variance (%)
East	Semi-diurnal	5	1	81.47	0.42	99.48
			2	109.59	4.51	95.88
			3	81.27	3.74	95.40
			4	146.23	0.71	99.51
			5	260.38	1.09	99.58
North	Semi-diurnal	5	1	15.94	0.14	99.12
			2	16.89	8.19	51.51
			3	15.88	2.23	85.96
			4	20.31	0.29	98.57
			5	38.37	1.31	96.59
East	Semi-diurnal	3	1	175.73	0.17	99.90
			2	97.43	3.23	96.68
			3	79.05	0.42	99.47
			4	147.75	0.70	99.53
			5	111.30	54.72	50.84
North	Semi-diurnal	3	1	21.96	0.21	99.04
			2	13.10	7.23	44.81
			3	12.89	0.89	93.10
			4	19.96	0.31	98.45
			5	16.20	5.19	67.96
East	Semi-diurnal	1	1	144.75	0.30	99.79
			2	44.16	19.44	55.98
			3	18.53	12.90	30.38
			4	140.62	1.98	98.59
North	Semi-diurnal	1	1	19.50	0.12	99.38
			2	7.52	7.52	0.00
			3	13.37	4.64	65.30
			4	14.30	1.78	87.55

Table 7. Reference current harmonic constants from BC-4 (58°37'N, 168°14'W) used in the response tidal analyses of the current data from the mid-shelf station BBL2.

Constit.	Period (hours)	Amplitude (cm/s)	Greenwich Phase Lag (°G)	Amplitude Ratio	Relative Phase Lag (°)
Q1	26.87	1.3	320	0.111	-30
O1	25.82	7.4	330	0.632	-20
M1	24.84	0.4	340	0.034	-10
P1	24.07	3.8	348	0.325	-2
K1	23.93	11.7	350	1.000	0
J1	23.10	0.7	0	0.060	10
001	22.31	0.4	10	0.034	20
2N2	12.91	1.8	332	0.066	-146
μ2	12.87	1.6	342	0.059	-136
N2	12.66	9.6	45	0.352	-73
υ2	12.63	1.0	55	0.037	-63
M2	12.42	27.3	118	1.000	0
L2	12.19	0.4	191	0.015	73
T2	12.02	0.1	249	0.004	131
S2	12.00	1.5	254	0.055	136
K2	11.97	0.4	265	0.015	147

Table 8. Current harmonic constants for O1, K1, N2, M2 from the current meter data at the mid-shelf station BBL2 (57°37'N, 167°45'W; 69m depth) obtained by the response method (1 complex weight per tidal band; 207 hour series length) with predicted tidal currents at BC-4 (Table 1) as the reference. The labels (8201) and (8202) on the values for the height of 5m refer to the two moorings at the station.

Constit.	Height (m)	Amplitudes Major (cm/s)	Amplitudes Minor (cm/s)	Greenich Phase Lag[1] (°G)	Orientation of Major Axis (°True)	Sense of Rotation[2]
O1	30	(7.0)	(1.3)	(140.8)	(285.1)	c
	15	7.3	3.3	133.8	293.6	c
(8201)	5	7.5	2.9	133.8	298.5	c
(8202)	5	7.3	2.8	133.3	295.5	c
	3	5.8	2.7	132.8	298.2	c
	1	5.7	2.3	132.2	289.7	c
K1	30	(11.1)	(2.0)	(160.8)	(285.1)	c
	15	11.5	5.2	153.8	293.6	c
(8201)	5	11.8	4.6	153.8	298.5	c
(8202)	5	11.6	4.4	152.3	295.5	c
	3	9.2	4.2	152.8	298.2	c
	1	9.0	3.7	152.2	289.7	c
N2	30	(7.9)	(6.0)	(16.2)	(28.9)	c
	15	7.8	5.9	19.2	43.2	c
(8201)	5	7.6	5.9	12.0	40.5	c
(8202)	5	7.5	5.8	14.6	43.5	c
	3	6.2	4.7	14.6	42.9	c
	1	5.8	4.4	12.1	33.7	c
M2	30	(22.6)	(17.2)	(89.2)	(28.9)	c
	15	22.1	16.9	92.2	43.2	c
(8201)	5	21.5	16.9	85.0	40.5	c
(8202)	5	21.2	16.4	87.6	43.5	c
	3	17.6	13.3	87.6	42.9	c
	1	16.5	12.5	85.1	33.7	c

[1] Major Axis
[2] c=clockwise

The reductions in variance (Table 9) for BBL2 are quite good with the exception of the 30m record. This is further evidence of a problem in this record. The reductions in variance (Table 9) for BBL2 are better than those (Table 3) for BBL1. One reason for this difference may be the choice of reference series. Predicted tidal currents from a nearby station were used as the reference series for BBL2 whereas predicted tides were used for BBL1. For the mid-shelf station BBL2, tidal currents were chosen for the reference because of tidal amphidrome regions (Fig. 3) of a small tidal amplitudes and rapidly changing phase near the station. Tides were chosen as the reference for the coastal station BBL1 because it is located in a relatively simple tidal regime where the tides and tidal currents have similar characteristics. In such a regime it is often preferable to use tides for the reference because their harmonic constants are better determined due to a superior signal-to-noise ratio in the observations. The reference tidal station BC-2 (Fig. 1) is about 130km to the northwest of BBL1. This may be a sufficient distance for differences to appear in the tidal characteristics. Besides the influence of the reference series or the reduction in variance, the background noise level may also be a factor. The observations at BBL1 were made in May which is a stormier period than late July to early August when the BBL2 observations were made. Whatever the reasons for the differences in the reduction in variance between BBL1 and BBL2, the reductions are quite good for both station; and we may assume that the associated harmonic constants are adequate to calibrate the profile model.

Table 9. Reductions in variance as a result of response tidal analyses applied to the current time series at the mid-shelf station BBL2. Small residual variances and reductions near 100% indicate that almost all the variance in a given tidal band is accounted for by the predicted tidal currents resulting from the response method. The labels (8201) and (8202) and the values for the height of 5m refer to the two moorings at the station.

Component	Tidal Band	Height (m)	Variance Predicted $(cm/s)^2$	Variance Residual $(cm/s)^2$	Reduction in Variance (%)
East	Diurnal	30	104.23	2.20	97.89
		15	98.20	0.05	99.95
	(8201)	5	97.28	0.09	99.91
	(8202)	5	97.50	0.12	99.88
		3	60.37	0.02	99.97
		1	63.50	0.03	99.95
North	Diurnal	30	9.80	1.06	89.18
		15	40.84	0.10	99.76
	(8201)	5	44.32	0.07	99.84
	(8202)	5	38.16	0.15	99.61
		3	30.11	0.07	99.77
		1	19.70	0.06	99.70
East	Semi-	30	164.36	2.60	98.42
	Diurnal	15	182.31	1.58	99.13
	(8201)	5	170.19	1.13	99.34
	(8202)	5	168.44	1.54	99.09
		3	111.48	0.71	99.36
		1	88.95	0.61	99.31
North	Semi-	30	224.42	3.17	98.59
	Diurnal	15	185.33	1.98	98.93
	(8201)	5	183.19	1.97	98.92
	(8202)	5	173.20	2.28	98.68
		3	116.92	1.25	98.93
		1	111.72	1.23	98.90

4. CALIBRATION OF THE PROFILE MODEL

The model was tuned to observations in two steps. The first step was to choose the type of theoretical tidal wave that best resembled the observed tides and tidal currents at a given station. The second step was to fit the theoretical profiles of that wave to the observed tidal ellipses by varying parameters in the model.

a. Wave Type

The appropriate type of tidal wave for each station was determined from the observed distributions of tidal currents (Fig. 2) and tides (Fig. 3). The coastal station BBL1 (56°19'N, 161°33'W) is located (Fig. 1) near the Alaska Peninsula where the tidal ellipses (Tables 2 and 4, Figs. 2 and 4) are narrow and oriented parallel to the adjacent coast. The tidal amplitudes (Fig. 3) decrease seaward from the Alaska Peninsula, and the phase lags increase with distance away from the shelfbreak. The characteristics of the tidal ellipses and distribution of tides suggest that the tidal motions at BBL1 are associated with Kelvin waves (Pearson, Mofjeld and Tripp, 1981) trapped to the Alaska Peninsula and propagating away from their source in the deep Aleutian Basin of the Bering Sea.

BBL2 (57°37'N, 167°45'W) was deployed in the mid-shelf regime where the tidal ellipses (Figs. 2 and 4) are broad. The major axes of the M2 ellipses are oriented toward the northeast while the major axis of the narrower K1 ellipses are oriented toward the northwest. The amplitudes of tides (Fig. 3) are relatively uniform near BBL2. The M2 cophase lines (Fig. 3) are oriented toward the northwest over this regime although the M2 phase tends to be relatively constant in the region located northeast of BBL2. The K1 cophase

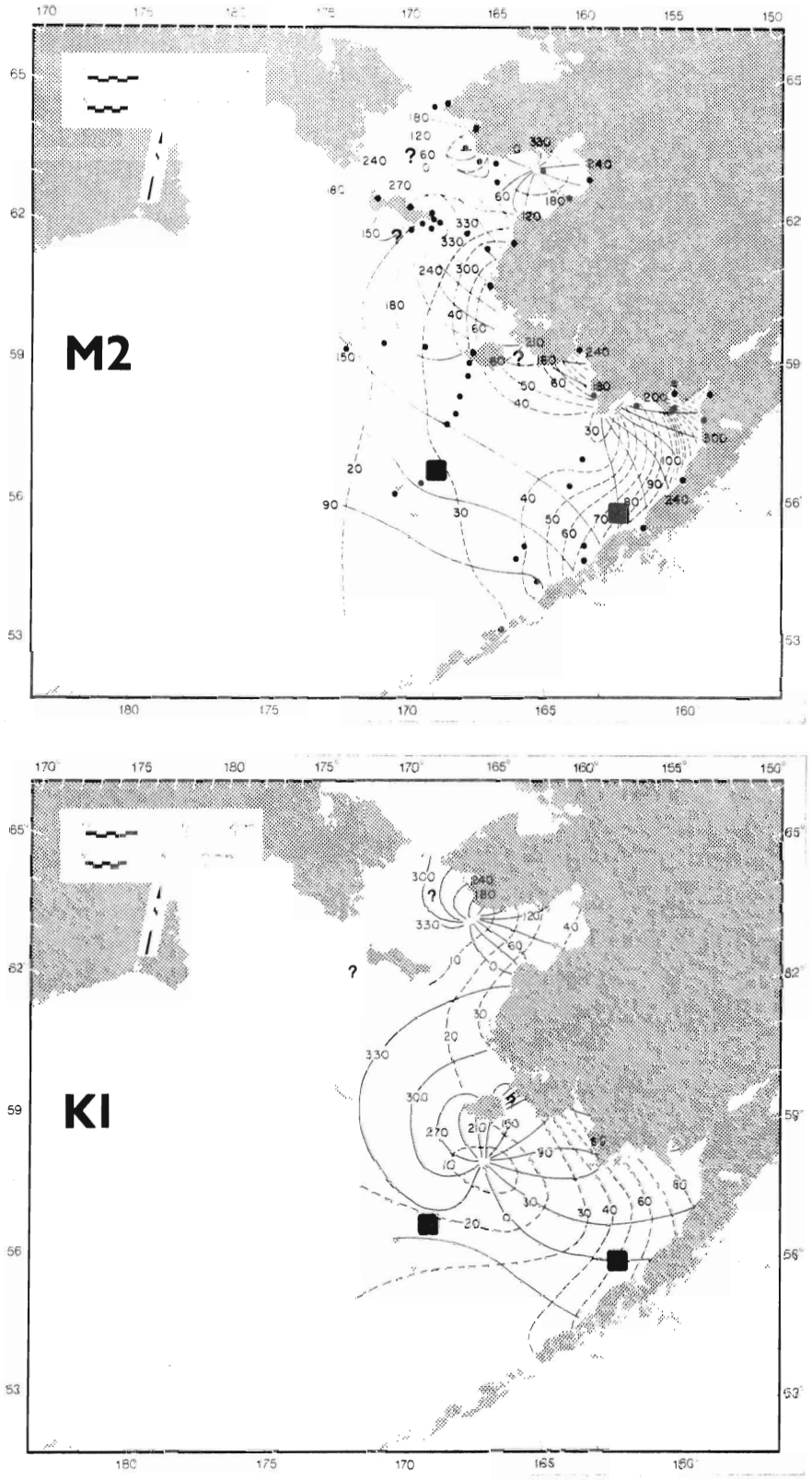

Figure 3. Empirical M2 and K1 cotidal charts for the Eastern Bering Sea Shelf. Solid lines are cophase lines and are labelled in degrees elapsed since Greenwich transit of the tidal constituent. Dashed lines are coamplitude lines and are labelled in centimeters of seawater. Dots in the M2 chart show the locations of observations used in the construction of the cotidal charts. Solid squares show the location of the bottom boundary layer stations BBL1 and BBL2. Modified from Pearson, Mofjeld and Tripp (1981).

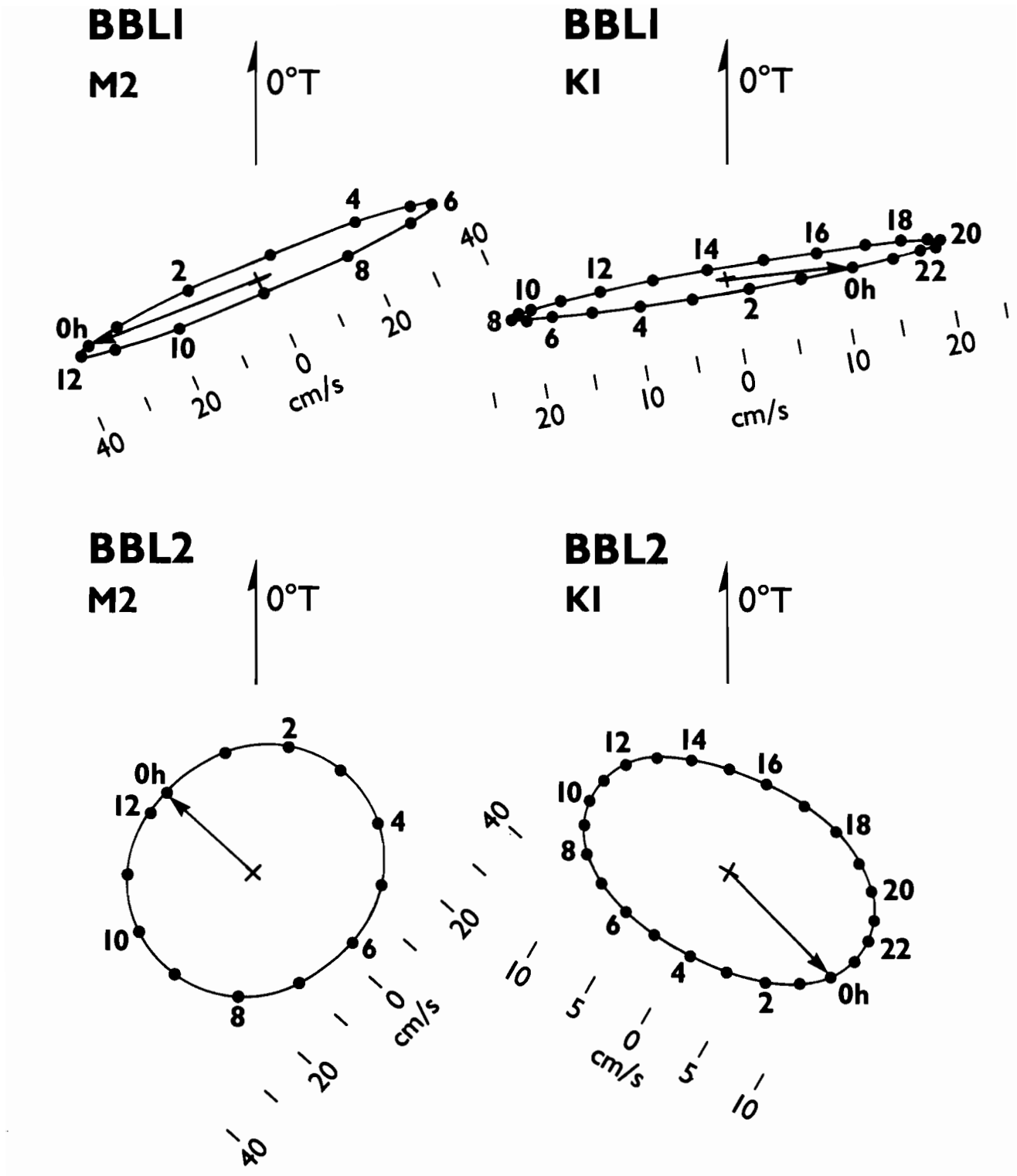

Figure 4. Representative M2 and K1 tidal ellipses at the bottom boundary layer stations BBL1 and BBL2. Dots on the ellipses show the tips of the velocity vectors are at hourly intervals and are labelled in hours elapsed since Greenwich transit for the tidal constituent. The orientation is relative to true north (0°T), and amplitude scales are shown in cm/s.

lines (Fig. 3) form a more complicated pattern. Near BBL2, a K1 cophase line is shown (Fig. 3) oriented toward the northwest, but the cophase lines to the north and east help form the radiating pattern of the K1 amphidrome located south of Nunivak Island.

The tidal ellipses and tides around BBL2 suggest that the tidal motions are due in part to Sverdrup waves propagating from the Aleutian Basin. Other waves suppliment the tidal motions as well. In the case of M2, the relatively constant phase (Fig. 3) to the northeast of BBL2 suggests that the incident Sverdrup wave reflects at the coast of Alaska. The northeastward progression of M2 phase lag (Fig. 3) on the outer shelf indicates that the incident M2 wave amplitude is larger than that of the reflected M2 wave near BBL2.

The K1 tidal motions at BBL2 are also due to a combination of waves. One K1 wave is that incident from the Aleutian Basin. It and the other waves form the amphidromic system (Fig. 3) south of Nunivak Island. The mid-shelf station BBL2 appears (Fig. 3) to be in the transition between the other shelf regime dominated by the incident K1 Sverdrup wave and the inner region of the K1 amphidromic system.

In choosing the appropriate wave type, it is helpful to compare quantitatively the observed tidal currents with those inferred from the tides using formulas based on inviscid theoretical waves. If the inferred current harmonic constants resemble closely the observed values at BBL1 and BBL2, then the tidal currents can be represented by a single wave of the appropriate type for each tidal constituent.

The comparison for K1 and M2 is presented in Table 10. In general, there is good agreement (Table 10d) between the inferred and observed values. For BBL1, the Kelvin wave formulas (Table 10a) yield narrow ellipses with amplitudes and orientation similar to the observations. The M2 phase lags

Table 10. Comparison of inviscid Kelvin waves at BBL1 and inviscid Sverdrup waves at BBL2 with observed K1 and M2 current harmonic constants above the bottom boundary layers. Theoretical currents are inferred from the tidal harmonic constants (Fig. 3).

a. Theoretical relations between the tide η and tidal currents with tidal amplitude η and phase lag $\eta°$

Wave Type	Amplitude Major	Amplitude Minor	Phase Lag	Orientation of Major Axis[1]	Sense of Rotation
Kelvin	$\sqrt{g/H}$	0	η	Perpendic.	—
K1 Sverdrup	$\frac{\sqrt{g/H}}{(f^2/\omega^2 - 1)^{\frac{1}{2}}}$	$\frac{\omega}{f}$ x Major	$\eta + 180°$	Parallel	C
M2 Sverdrup	$\frac{\sqrt{g/H}}{(1 - f^2/\omega^2)^{\frac{1}{2}}}$	$\frac{f}{\omega}$ x Major	η	Perpendic.	C

[1] Relative to the local cophase lines of the tide

b. Tidal harmonic constants (from Fig. 3)

Station	Constit.	Amplitude (cm)	Greenwich Phase Lag (°G)	Orientation of cophase lines[2] (°True)
BBL1	K1	51	358	330
	M2	80	180	330
BBL2	K1	20	335	310
	M2	31	135	290

[2]For BBL1, perpendicular to the general trend of the adjacent coast

c. Parameters used in theoretical relations

$g = 9.8\ m/s^2$ $\quad \omega(K1) = 7.29(10)^{-5}\ s^{-1}$ $\quad \omega(M2) = 1.405(10)^{-4}\ s^{-1}$

Station	Depth H (m)	$\sqrt{g/h}$ (s^{-1})	Latitude (°N)	f (s^{-1})
BBL1	63	0.394	56°19'	$1.213(10)^{-4}$
BBL2	69	0.377	57°37'	$1.231(10)^{-4}$

Table 10

d. Current harmonic constants

Constit.	Amplitude Major (cm/s)	Amplitude Minor (cm/s)	Amp. Ratio	Greenwich Phase Lag (°G)	Phase Diff. (°)	Orientation (°True)	Sense of Rotation
Station BBL1							
K1 (Obs.)	22	0.3	0.01	310	48	76	CC
K1 (Kelvin)	20	0	0	358		60	--
M2 (Obs.)	37	2	0.05	173	7	64	C
M2 (Kelvin)	32	0	0	180		60	--
Station BBL2							
K1 (Obs.)	12	5	0.42	154	1	298	C
K1 (Sverd.)	6	4	0.59	155		(290)	C
M2 (Obs.)	22	17	0.77	92	43	42	C
M2 (Sverd.)	24	21	0.88	135		40	C

agree, but the observed K1 phase lag is 48° earlier than the phase lag based on the assumption that the K1 current is in phase with the K1 tide. The K1 currents must therefore be the sum of at least two waves. From the K1 tidal distribution in Fig. 3, it seems that the K1 tides at BBL1 are under the influence of the K1 amphidromic system. In particular, the K1 distributions to the north and northeast of BBL1 form the classic pattern of a Kelvin wave propagating around an embayment. The K1 phase difference (Table 10d) at BBL1 indicates that the influence of the K1 motion propagating northwestward along the northeast coast extends to BBL1. This is not the case for the M2 tide (Fig. 3) where the influence of the virtual (on land) amphidrome extends only as far as Kvichak Bay.

The quantitative comparison (Table 10d) between Sverdrup and observed tidal currents at the mid-shelf station BBL2 reveals generally good agreement with some important exceptions. As with the theoretical currents at BBL1, the theoretical estimates of the tides (Table 10c) from the cotidal charts in Figure 3. Different formulas are used for K1 and M2 because Sverdrup waves change character as the frequency passes through the inertial frequency f.

The M2 Sverdrup amplitudes (Table 10d) at the mid-shelf station are in good agreement with the observations except that the amplitude ratio of minor to major axes is somewhat larger for the M2 Sverdrup wave (0.88) than for the observed M2 current (0.77). The inferred K1 current has an amplitude (6 cm/s) along the major axis which is half the observed value (12 cm/s). This discrepancy may be due to the inference of the K1 amphidromic system (Fig. 3) near BBL2 since regions within such systems can have much larger currents than those inferred from the local tides under the assumption that the currents are due to a single wave. The amplitude ratio (0.59) of the K1 Sverdrup wave is larger than that observed (0.42).

Turning to the phase lags (Table 10d) at BBL2, there is excellent agreement between the K1 Sverdrup and observed phase lags. Evidently, the phase lag of K1 at the mid-shelf station BBL2 is controlled by the incident K1 Sverdrup wave even though the K1 amplitude at BBL2 is strongly affected by the K1 amphidromic system. It appears that BBL2 is located in the transition between two K1 tidal regimes - one dominated by the incident K1 Sverdrup wave and the other associated with the K1 amphidromic system (Fig. 3) to the east and north of BBL2. The M2 phase lags (Table 10d) at BBL2 show less agreement. The earlier M2 phase lag of 43° in the observations relative to the theory suggests that there is a reflected Sverdrup wave at BBL2 propagating southwestward from the Alaskan coast, in addition to the incident M2 Sverdrup wave from the Aleutian Basin. If the two waves had equal amplitudes, the M2 current observations would lead those based on the local tide by 90°. The fact that the actual M2 phase lead is 43° suggests that the incident M2 Sverdrup wave is dominant but that the reflected wave is significant.

The theoretical orientations (Table 10d) of the tidal ellipses at BBL2 agree relatively well with those observed. The assumption that the theoretical K1 and M2 tidal currents are associated with Sverdrup waves also produces the large difference in orientation observed (Fig. 2) between these tidal constituents. The theoretical and observed orientations are consistent with those for the mid-shelf region. The major axes of the M2 ellipses are oriented toward the northeast, which is parallel to the direction of propagation for the M2 wave incident from the Aleutian Basin. The K1 ellipses are oriented to the northwest, which is perpendicular to the incident direction of the K1 wave. The simple theory predicts the correct clockwise rotation is expected in the mid-shelf region where the Coriolis effect can

accelerate moving water to the right without the inhibiting influence of a nearby coast.

The comparison of simple waves with the observed tidal currents is helpful in understanding the tidal dynamics at the two stations and in contrasting the differences in the tidal currents at the coastal BBL1 and mid-shelf BBL2 stations. It also serves to show that the simple Kelvin and Sverdrup waves explain many of the observed tidal features but that there are some differences between the tidal currents predicted from the tides using these waves and the currents observed at the stations. This will be important to keep in mind when we interpret the residual tidal currents based on the waves.

b. Fit of Model Parameters

Having chosen the wave type for each station, we proceed to fit theoretical profiles of currents to the observed profiles of tidal ellipses for the K1 and M2 tidal constituents. The tides do not play a direct role in the calibration of the profile model as they did in the discussion on wave type. Instead, the model is fitted directly to the observed tidal ellipses. There are several parameters in the model that can be adjusted. The amplitude, phase lag and orientation of K1 and M2 currents can be varied at one height in the water column. The bottom roughness length z_o can also be varied. The model then produces continuous profiles over the entire water column which pass through the values at the reference height. The amplitude ratio of minor to major axes is determined by the frequency ω of the tidal constituent, the Coriolis parameter f and the wave type.

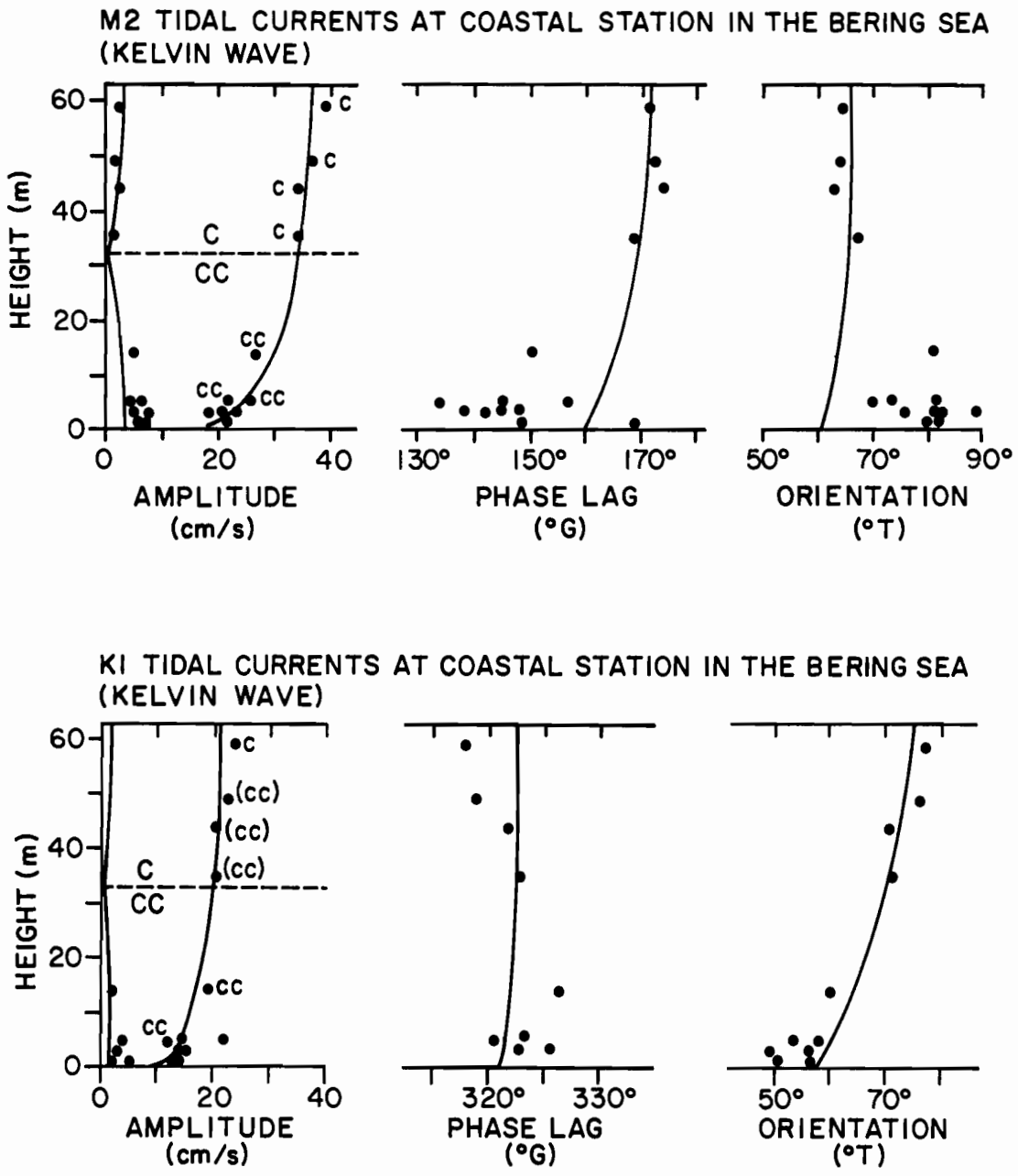

Figure 5. Fit (solid lines) for BBL1 of the profile model to observed M2 and K1 tidal ellipse elements (dots): amplitudes along the major and minor axes, Greenwich phase lag and orientation. The symbols c and cc refer to clockwise and counterclockwise senses of rotation respectively. The dashed lines show the location in the water column where the profile model predicts the transition from clockwise to counterclockwise rotation should occur.

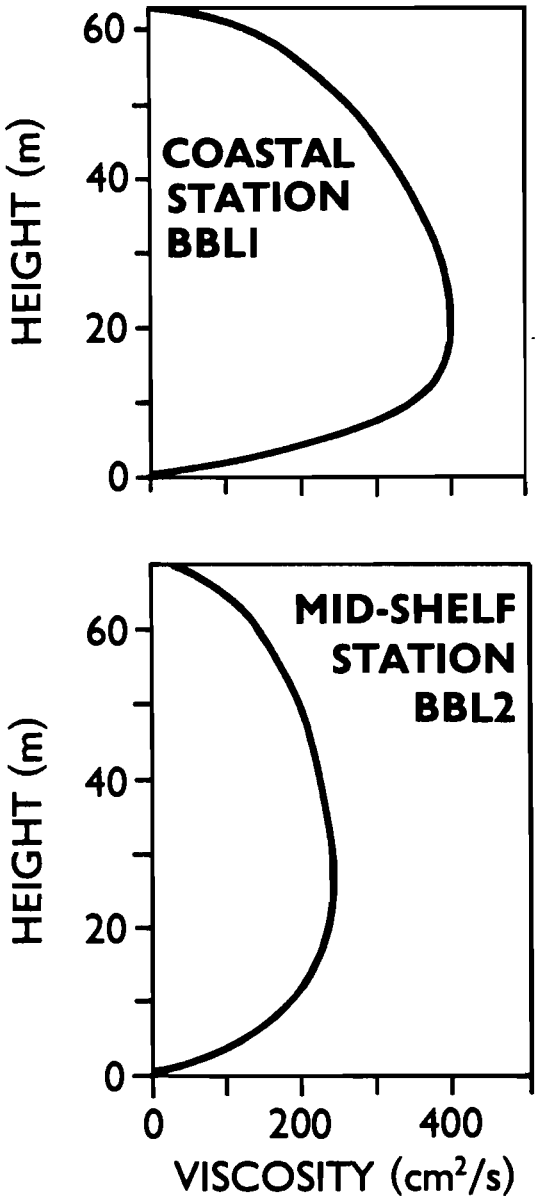

Figure 6. Theoretical profiles of eddy viscosity corresponding to fits (Figs. 5 and 7) of the profile model to the observed tidal currents at BBL1 and BBL2. These viscosities are sums of those generated by the major tidal constituents O1, K1, N2 and M2.

The strength of the viscosity is determined in part by the bottom roughness length z_o which is adjusted to match the shear profiles in the bottom boundary layer. Changing the amplitudes of the tidal currents also changes the profile of viscosity. Fitting the model to the observations becomes an iterative process in which the constituent parameters and roughness length z_o are adjusted in turn. The result of the fit at each station is a compromise between matching the vertical profiles of amplitude, phase lag and orientation. We have placed primary emphasis on matching the amplitude profiles.

The theoretical K1 and M2 profiles for the coastal station BBL1 are shown in Fig. 5 together with the observed values from Tables 2 and 4. Not all the observed values were plotted for the near-bottom meters at 1, 3 and 5 m heights; only those values in Table 4 were used which corresponded to relatively good reductions in variance. Nevertheless, there is still considerable scatter in the near-bottom observations.

The profile model reproduces several of the features seen in the observations. These include the shapes of the amplitude profiles and the height at which the sense of rotation switches for M2 from counterclockwise below to clockwise above. The observed sense of rotation for K1 is not statistically significant at mid-depth because of noise affecting the small K1 amplitudes along the minor axis.

The fit of the profile model to the observed amplitude profiles required at the coastal station BBL1 a large viscosity (Fig. 6a). This in turn requires an unusually large value for the roughness length z_o = 1.0 cm; the implied vertical scale of the roughness elements is then 30 cm. One explanation for such a large z_o has to do with the effect of surface swell on the bottom boundary layer.

As pointed out by Grant and Madsen (1979), surface swell create a thin boundary layer just above the bottom which has the same effect on low-frequency motions like tidal currents as enhanced bottom roughness. If the large apparent roughness at BBL1 were due to surface swell, the roughness and hence the profiles of tidal currents would depend on the intensity of the swell which varies through the seasons of the year. Whether this is true cannot be demonstrated in the observations at BBL1 since no swell measurements were made during the period of observation at BBL1. It is known from shipboard observations however that the current observations at BBL1 were taken during a stormy period. Another explanation for the large roughness is that there were bedforms at the surface of the bottom sediment with amplitudes of the order of 30 cm. It is not known whether substantial bedforms existed at BBL1 during the period of observation.

The theoretical profiles (Fig. 5) of phase lag at BBL1 do not match the details of the observations. The theoretical K1 phase lag is essentially constant over the water column except for a small decrease (~3°) from the 20 m height to the bottom. The observed K1 phase lag has much more structure over the water column. The observed phase lag increase by 16° from the surface to the 14 m height and then decreases by ~6° from that height to the bottom. Crean (private communication, 1982) has found from 3-dimensional tidal models of the Straits of Juan de Fuca-Georgia that non-linear interactions between the tidal constituents can induce large vertical variations (as much as 100°) in K1 phase lag. It may be that the vertical structure (Fig. 5) of K1 phase lag at BBL1 is controlled by non-linear interaction not included in the profile model. The theoretical profile (Fig. 5) of M2 phase lag shows the correct tendency for earlier (smaller) phase lag moving downward in the water column but the theoretical profile underestimates the total phase shift, a factor of about 2 (11° versus 24°).

The K1 orientations (Fig. 5) of the model and observations agree rather well at BBL1. Both show a counterclockwise rotation of K1 ellipses moving downward from the surface. The theoretical profile (~17°) does underestimate the observed change (~24°) over the water column. The theoretical M2 profile of orientation is a poor match to the observations. The theory predicts a small (7°) counterclockwise rotation with depth whereas the observations indicate a clockwise rotation of ~16°. We have no explanation for this discrepancy in M2 orientation at this time; possible explanation may be related to topographic effects which are not included in the model.

Turning to the fit (Fig. 7) of the profile model to the observations at the mid-shelf station BBL2, we see that the reliable observations (Table 8) are confined to the bottom 15 m of the water column. It isn't possible to check the model well-above the bottom boundary layer as is the case for the coastal station BBL1.

The near-bottom profiles (Fig. 7) of amplitude for the model can be matched relatively easily to the observations at BBL2. The major increases in amplitude occur closer to the bottom than is the case (Fig. 5) for the coastal station BBL1. This is suprising because a Sverdrup wave regime such as that at the mid-shelf station BBL2 should have a relatively thick bottom boundary layer due to the dominance of the clockwise-rotating velocity components. For the same profile of viscosity, the Kelvin waves would have a thinner bottom boundary layer. The key to the difference is amplitude profiles between the two stations BBL1 and BBL2 must lie in the differences in viscosity (Fig. 6). To fit the amplitude observations (Fig. 7) at BBL2 requires a small value of the bottom roughness length z_o (0.001 cm). This small value of z_o combines with the relatively smaller current amplitudes at BBL2 to produce a less intense viscosity (Fig. 6) than at BBL1. The differences

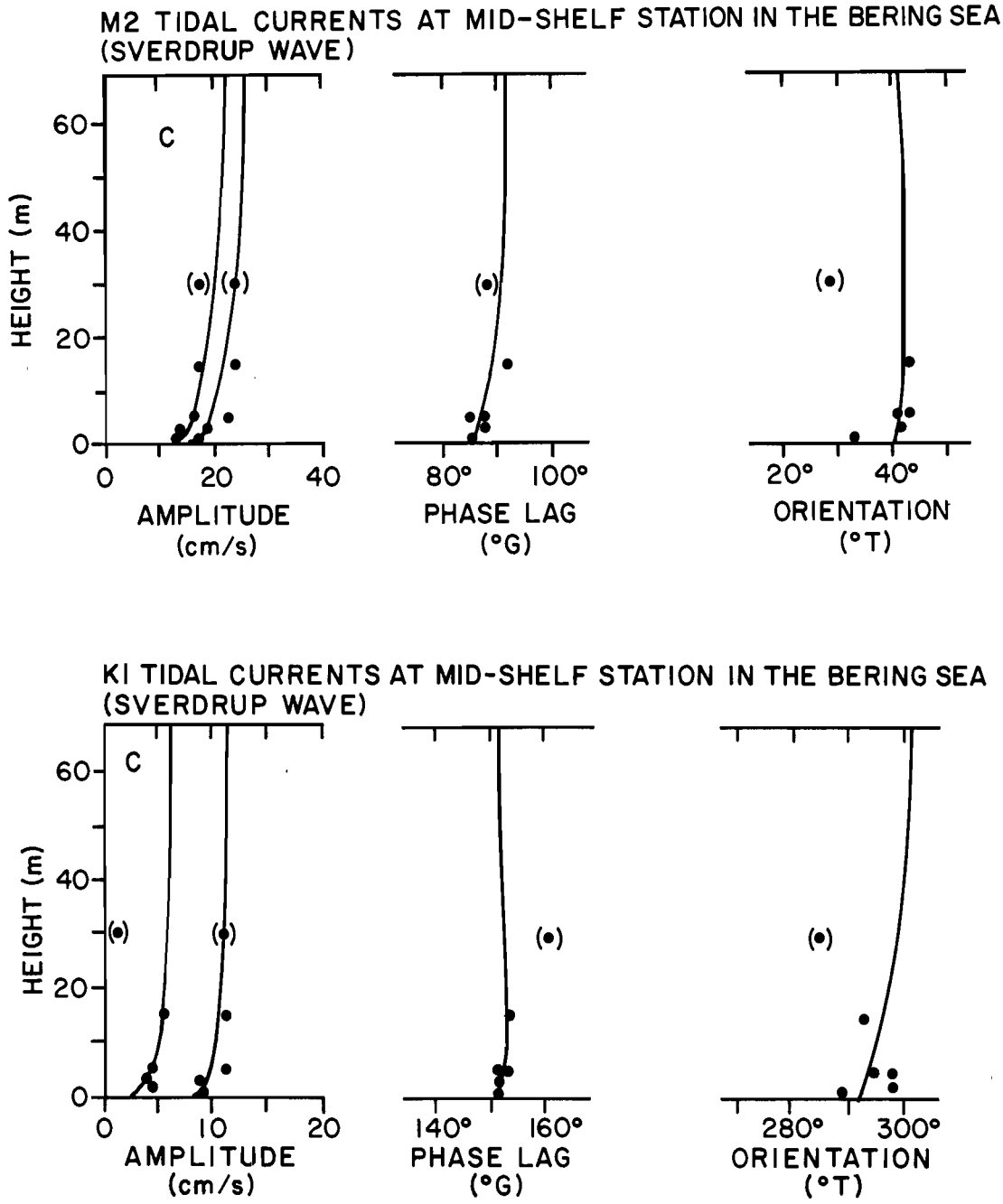

Figure 7. Fit (solid lines) for BBL2 of the profile model to observed M2 and K1 tidal ellipses elements (dots): amplitudes along the major and minor axes, Greenwich phase lag and orientation. The symbol c near the amplitude curves indicates that the sense of rotation is clockwise for both the theoretical and observed ellipses. The observed values at the 30 m height are in parentheses because the current meter was defective.

in viscosity between the two stations is sufficient to overcome the opposing tendency due to the differences in wave type. One reason for this smaller z_o inferred at BBL2 may be that the observations were taken at a quieter time of year (late August-early September) for surface swell than was the case at BBL1 (May). Shipboard observations suggest that this was indeed the case.

Tidal theory predicts that an M2 Sverdrup wave at high latitude should have nearly circular ellipses and thicker bottom boundary layers than K1. At the mid-shelf station BBL2, the K1 ellipses (Fig. 7) are narrower (smaller relative amplitude along the minor axes) and the K1 bottom boundary layer thinner than is the case for the M2 ellipses at BBL2. The direct fit (Fig. 7) of the profile model to K1 currents matches the amplitude ratios of the K1 Sverdrup wave and observations (though this did not occur when the K1 Sverdrup currents were computed from the local K1 tide as shown in Table 10).

The vertical variations of the theoretical and observed phase lags (Fig. 7) agree well at BBL2. They show that the K1 phase lag is nearly constant over depth while the M2 phase lag is smaller (~6°) than that above the bottom boundary layer. The observations of K1 orientation at BBL2 shows considerable scatter, and it is difficult to test the validity of the counter-clockwise trend of the theoretical K1 orientation. The observed K1 and M2 orientation at the 1m height deviate in the same way and by the same amount from the corresponding observations at 3 and 5 m. This may be due to the effect of the steel anchor and its associated magnetic field on the magnetic compass of the current meter at the 1 m height. If the observed orientation at 1 m are rejected, the theoretical K1 profile of orientation has the wrong trend with height. This is a tenuous finding because it is based in large part on the single value at the 15 m height.

A few summary remarks seem appropriate for this section. Matching the profile model to the observations at BBL1 and BBL2 was done in two steps. The first step was to identify the best wave type for each station. This was relatively easy because the station locations were purposely chosen to lie in tidal current regimes that resembled either the Kelvin or the Sverdrup waves. The study of how the local tides relate to the tidal currents showed the similarities of the observations to the simple waves as well as the differences between the actual currents and those based on this simple theory. Fitting the model to the observed profiles of K1 and M2 currents was the second step. There are actually relatively few parameters to adjust in the model. One of these is the bottom roughness parameter which turned out to be quite different at the two stations. The reasons for the difference is a matter of speculation. The inability of the model to reproduce some of the profiles of the tidal ellipse parameters shows that there are processes at work which are not included in the model. To understand the tidal currents in detail will require a more complete model that includes non-linear interactions between the tidal constituents and bottom topography.

5. RESIDUAL TIDAL CURRENTS

The residual tidal currents computed from the profile model represent only part of the residual flow induced by tidal motions. They are that part generated locally by simple wave analogs propagating over a horizontal bottom. The computations do not take into account non-linear interactions between tidal constituents, effects of topography nor residual tidal currents generated in other tidal regimes that flow into the region. The model also ignores the difference between the actual tidal motions and those due to the simple Kelvin and Sverdrup waves. Even though the profile model cannot produce realistic estimates of the *complete* residual tidal currents, it allows considerable insight into the processes that give rise to the residual currents and shows the differences between the two tidal regimes where the observations were made. It also shows that the mass transport generated by tidal currents can be quite different from a simple time-average of local currents.

It is helpful to first consider residual currents based on waves without friction. Simple expressions (Table 11a and b) can be written for these waves which show explicitly the relative importance of wave type, amplitude, frequency and total depth in determining the speed and direction of the residual currents. Estimates (Table 11c) from these expressions are consistent with the residual tidal currents (Figs. 8 and 9) above the bottom boundary layer based on waves subject to viscosity.

The inviscid Kelvin waves at the coastal station BBL1 each generate a Stokes drift (Table 11b) in the direction of propagation but their Eulerian current has zero speed. The quadratic dependence (Table 11b) of the Stokes drift on amplitude causes the largest constituent M2 to dominate the residual

Table 11. Theoretical estimates of K1 and M2 residual tidal currents at the coastal station BBL1 and mid-shelf station BBL2 based on inviscid Kelvin and Sverdrup waves, respectively. The currents are independent of height.

a. Theoretical Equations (propagation in the y-direction)

	Stokes	Eulerian	Lagrangian
x-component	$u_S = \overline{\Delta Y \frac{\partial u}{\partial y}}$	$fu_E = -\overline{v\frac{\partial v}{\partial y}}$	$u_L = u_S + u_E$
y-component	$v_S = \overline{\Delta Y \frac{\partial v}{\partial y}}$	$-fv_E = -\overline{v\frac{\partial u}{\partial y}}$	$v_L = v_S + v_E$

b. Theoretical Expressions

Wave Type	Stokes Speed	Stokes Dir.	Eulerian Speed	Eulerian Dir.	Lagrangian Speed	Lagrangian Dir.
K1 & M2 Kelvin	$V^2/2C_o$	0°	0°	0°	←Vector Sum	
K1 Sverdrup	$(1-\omega^2/f^2)^{\frac{1}{2}}V^2/2C_o$	-90°	$\frac{\omega^2}{f^2}$ × Stokes	90°	←Vector Sum	
M2 Sverdrup	$(1-f^2/\omega^2)^{\frac{1}{2}}V^2/2C_o$	0°	Stokes	180°	←Vector Sum	

V = Amplitude along major axis; direction is relative to propagation direction

$C_o = \sqrt{gH}$

c. Estimates of Residual Tidal Currents (Observed parameters from Table 10)

Sta.	Constit.	Stokes Speed (cm/s)	Stokes Dir. (T°)	Eulerian Speed (cm/s)	Eulerian Dir. (°T)	Lagrangian Speed (cm/s)	Lagrangian Dir. (°T)
BBL1	K1 (Kelvin)	0.10	76	0	-	0.10	76
	M2 (Kelvin)	0.28	64	0	-	0.28	64
BBL2	K1 (Sver.)	0.022	298	0.008	118	0.014	298
	M2 (Sver.)	0.045	42	0.045	222	0	-

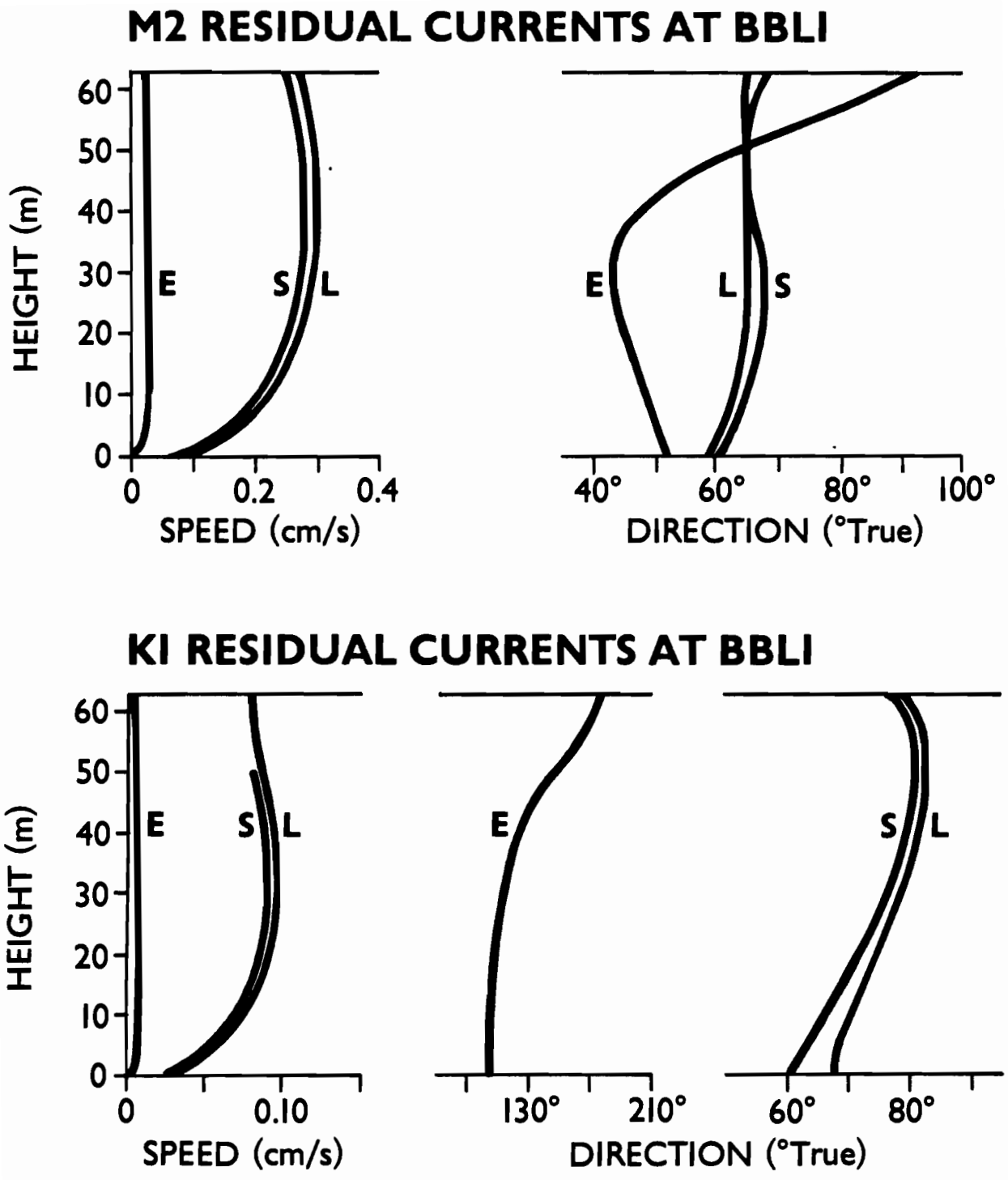

Figure 8. Theoretical M2 and K1 residual currents at BBL1 computed with the profile model. Shown are profiles of Eulerian current E, the Stokes drift S and the Lagrangian current L.

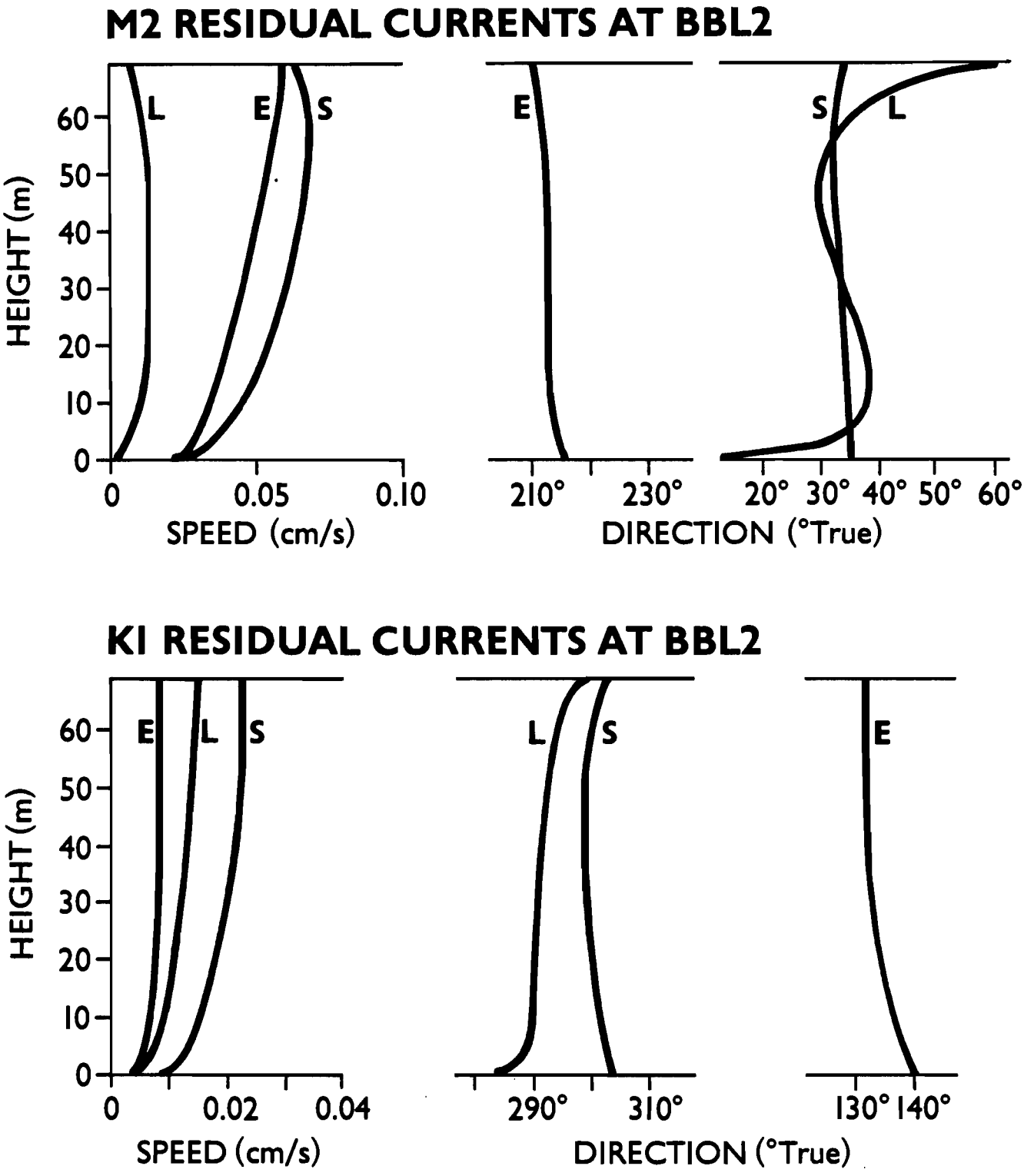

Figure 9. Theoretical M2 and K1 residual currents at BBL2 computed with the profile model. Shown are profilers of Eulerian current E, Stokes drift S, and Lagrangian current L.

currents (Table 11c). At BBL1, the estimated residual currents are on the order of a few tenths of a cm/s. The magnitudes of these currents can be expected to increase shoreward from this station because the current amplitudes of Kelvin waves increase and the phase speed c_o decreases. Conversely, the residual currents should decrease seaward of BBL1.

At the mid-shelf station BBL2, inviscid Sverdrup waves produce non-zero Eulerian currents (Table 11) in addition to the Stokes drift. Indeed, the M2 Eulerian current is equal in speed but opposite the direction to the M2 Stokes drift. As a result, the net M2 Lagrangian current has a net zero speed; this is also true for the other semidiurnal constituents. As for the other diurnal constituents, the K1 residual current (Table 11) at BBL2 are dominated by the Stokes drift with a smaller contribution due to the Eulerian current. The directions of the K1 residual currents are perpendicular to the direction of propagation.

There are several reasons that the Stokes drifts and Lagrangian currents (Table 11) are smaller at the mid-shelf station BBL2 than at the coastal station BBL1. The most important of these is that the tidal current amplitudes (Table 10) are smaller at BBL2. Of next importance is that M2 Sverdrup waves have smaller tides (vertical excursions) than Kelvin waves for the same tidal current amplitude and this produces smaller Stokes drifts. Finally, the water depth is greater at BBL2 which produces a larger phase speed and hence smaller residual currents. The K1 waves at BBL1 and BBL2 are quite different. There is a propagating Kelvin wave at BBL1 and an evancescent (spatially decaying) Sverdrup wave at BBL2. The differences in K1 residual currents at the two stations are a reflection of this as well as the differences in amplitude and water depth at the two stations.

Vertical viscosity modifies the residual tidal currents. At the coastal station BBL1, the residual currents (Figs. 8 and 10) are still dominated by the Stokes drift with a very small Eulerian current (<0.03 cm/s) induced by dissipation along the direction of propagation. Because the tidal currents (Fig. 5) with friction vary in amplitude and orientation over the water column, the speeds and directions of the residual currents are also functions of height. The decrease in tidal currents near the bottom are responsible for the corresponding decrease (Figs. 8 and 10) in Stokes drift and Lagrangian current.

Based on a sum of contributions from the four major tidal constituents 01, K1, N2 and M2, the total Lagrangian currents at BBL1 has a maximum speed of about 0.4 cm/s and a direction along the coast away from the shelfbreak. This is probably an accurate estimate of the Stokes drift at BBL1 because the tidal currents flow parallel to isobaths with little topographic generation of residual currents. Sündermann (1977) found from a vertically-integrated model of M2 in the Bering Sea that Kvichak Bay is a major source of Eulerian residual flow for the Eastern Bering Sea Shelf. This outflowing Eulerian current finds its source in the incoming M2 Stokes drift.

The Stokes transport due to the M2 Kelvin wave near the Alaska Peninsula can be estimated by integrating the inviscid expression $v_S = V^2/2c_o$ in the seaward direction. We assume that amplitude V of the M2 tidal current decays exponentially with offshore distance with a decay distance c_o/f = 205 km and that the M2 amplitude equals the observed value (Table 10) at BBL1. The Stokes transport due to the M2 Kelvin wave is then approximately HV_o^2/f = 1.0 $(10)^5 m^3/s$ where H is 63 m and the current amplitude V_o at the coast is 44 cm/s based on an offshore distance of 37 km for the location of BBL1. The corresponding K1 Stokes transport is 0.4 $(10)^5 m^3/s$. The total Stokes

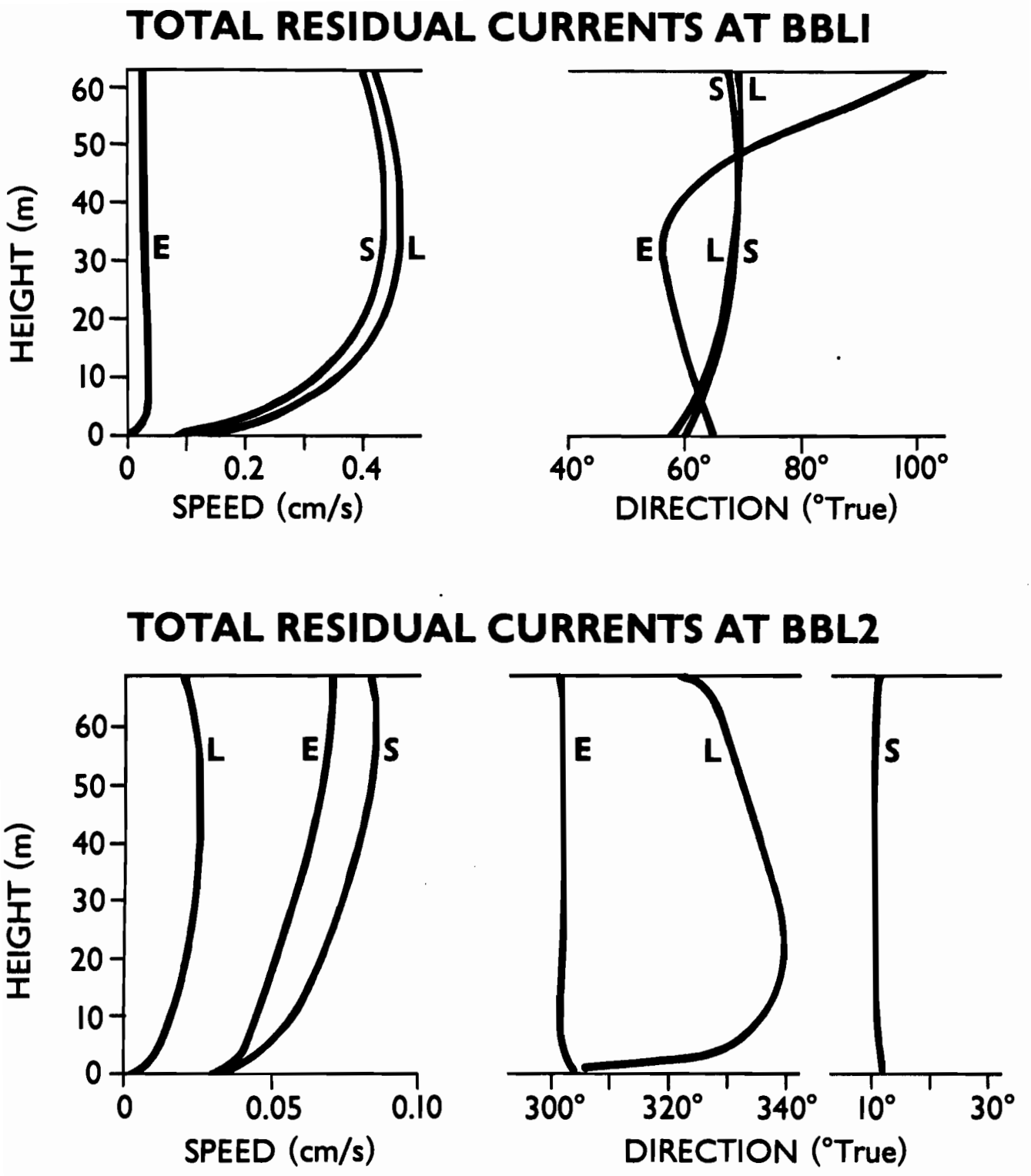

Figure 10. Total residual currents at BBL1 and BBL2 obtained by summing the contributions of the major tidal constituents O1, K1, N2 and M2. Shown are profiles of Eulerian current E, Stokes drift S, and Lagrangian current L.

transport in this region is about 1.7 $(10)^5 m^3/s$, based on the sum of O1, K1, N2 and M2 Stokes drifts. This transport is along the Alaska Peninsula toward the northeast. The corresponding Stokes drift speed decays seaward with a decay distance 102 km equal to half that of the inviscid Kelvin waves. The Stokes transport is therefore confined to a coastal band about 205 km.

Vertical viscosity also affects the theoretical residual currents (Figs. 9 and 10) at the mid-shelf station BBL2, but the general characteristics of these currents are the same as those (Table 11) without friction. There is still the tendency for the M2 Eulerian current to cancel the M2 Stokes drift, producing a small M2 Lagrangian current. The K1 residual current (Fig. 9) at BBL2 is dominated by the Stokes drift with a direction (~300°T) perpendicular to the direction of wave propagation. As with the inviscid currents, the total residual currents (Fig. 10) at BBL2 have considerably smaller speeds than those at the coastal station BBL1 because the tidal current amplitudes are less at BBL2, the wave type is Sverdrup and the water depth is greater than at BBL1. The maximum speed (Fig. 10) of the total Lagrangian current computed for BBL2 is only 0.02 cm/s, which is a factor of 20 smaller than that at the coastal station BBL1.

The residual currents at the mid-shelf station BBL2 are probably enhanced by topographically generated currents. A rough estimate of the M2 topographic currents can be obtained from the formulas.

$$u_S = 0 \ , \ v_S = - \frac{\alpha}{H} \frac{f}{\omega^2} \frac{V^2}{2} \ , \ u_E = - \frac{\alpha}{fH} \frac{V^2}{2} \ , \ v_E = 0 \qquad (35)$$

where α is the local slope of the bottom and the M2 wave is assumed to be propagating into shallow water. The formulas (35) are derived from the

equations in Table 11 under the assumption that the decrease in depth in the direction of propagation causes an increase in tidal current amplitude sufficient to conserve the instantaneous tidal transport. For a representative bottom slope $\alpha = 2(10)^{-4}$ and M2 parameters for Table 10, the M2 topographic residual current at BBL2 has a speed of 0.07 cm/s and a direction of 280°T. The topographic Stokes drift and Eulerian current do not cancel. Hence, the topographic current is comparable in magnitude with the M2 Stokes drift (Table 11) derived earlier and is larger than the Lagrangian current. Both topographic currents are small (<0.1 cm/s). They can however be larger where local topographic features produce larger bottom slopes (Schumacher and Kinder, 1983). The direction of this flow would be toward the west if isobaths are oriented toward the northwest.

The theoretical residual currents discussed in this section are helpful in understanding the generation of residual currents. They are however based on many assumptions. The Stokes drifts do represent the local residual currents of this type but the theoretical Eulerian currents should include currents flowing past the observation point from other tidal regimes. A model of the entire Eastern Bering Sea Shelf is required to do this adequately. From the vertically integrated model by Sündermann (1977) for M2 in the Bering Sea, it appears that the M2 Eulerian residual current (Fig. 11) is small (<1 cm/s) at the two stations BBL1 and BBL2. In this model, the only significant Eularian current flow is along the coast of Alaska toward the northwest. This current is primarily due to northeastward M2 Stokes drift of the M2 Kelvin wave propagating along the Alaska Peninsula (Fig. 3). This drift is converted into the Eulerian current in the shallow embayments of Bristol Bay.

6. SUMMARY

A classical analysis of tidal current profiles on the shelf has been extended to include a Level II turbulence closure treatment of the eddy viscosity. This removes a major ambiguity in the choice of the vertical scale for the viscosity. When a number of tidal constituents are present, each contributes to the composite, time-averaged viscosity. At present, the model is restricted to free waves propagating in unstratified water without ice cover. An important parameter in the model is the bottom roughness length, which can be determined by fitting theoretical profiles to observed current harmonic constants.

Detailed observations of tidal current profiles were made at two sites on the Southeastern Bering Sea Shelf to study the vertical structure of tidal currents in two distinctly difference tidal regimes. The rectilinear tidal currents at the coastal station BBL1 were observed to have thick bottom boundary layers with significant variations in speed and phase extending well up into the water column. Comparison with the Level II model indicates that the apparent bottom roughness was large at BBL1 during the period of observation. At the mid-shelf station BBL2 located between the Pribilof Islands and Nunivak Island, the rotary tidal currents had thin bottom boundary layers with a small apparent bottom roughness.

The difference in apparent bottom roughness at the two stations is probably due to the difference in weather during the periods of observation and/or to the presence or absence of bedforms. The vertical structure of the tidal currents at the two stations is dominated by the strengths of the currents and the bottom roughness. The type of tidal wave is of secondary importance in determining the vertical heights of the bottom boundary layers.

Theoretical estimates of residual tidal currents generated by simple tidal waves fitted to the observed tidal currents at BBL1 and BBL2 indicate that the residual tidal currents have small speeds (~0.4 cm/s) in the absence of bottom topography. Near the Alaska Peninsula, tidal Kelvin waves generate a mass transport of ~$2(10)^5 m^3/s$ toward Kvichak Bay. At the mid-shelf station BBL2, the Sverdrup waves produce very small residual currents (~0.2 cm/s). Local topography could increase these currents to 1 cm/s if the local bottom slope is sufficiently large as may occur near the 50 m isobath.

7. ACKNOWLEDGMENTS

The research described in this report was supported by the Minerals Management Service through interagency agreement with the National Oceanic and Atmospheric Administration, under which a multiyear program responding to needs of petroleum development of the Alaskan Continental Shelf is managed by the Outer Continental Shelf Environmental Assessment Program (OCSEAP) Office. Support was also provided by NOAA's Environmental Research Laboratories.

The authors wish to express their appreciation to the following people for their excellent support work: T. Jackson and W. Parker for preparation of instruments and moorings; J. Blaha and T. Jackson for deployment and recovery of equipment; L. Long, S. Wright, P. Moen and D. Kachel for processing of data; R. Whitney and L. Lu for editing and typing; and J. Register and V. Curl for drafting. The authors also wish to thank J.W. Lavelle for helpful discussions on swell-induced boundary layers.

Many of the results in this memorandum were presented at the XVIII General Assembly of the International Union of Geodesy and Geophysics (IUGG) during August 1983 in Hamburg FRG by H.O. Mofjeld and J.W. Lavelle in a paper entitled "Bottom Boundary Layer Studies in Tidally Dominated Regimes".

8. REFERENCES

Blackadar, A.K., 1962: The vertical distribution of wind and turbulent exchanges in a neutral atmosphere, J. Geophys. Res., 67, 3095-3120.

Businger, J.A., and S.P.S. Arya, 1974: Height of the mixed layer in the stably stratified planetary boundary layer. Advances in Geophysics, 18A, Academic Press, 73-92.

Defant, A., 1961: Physical Oceanography, Vol. II. Pergamon Press, 598 pp.

Dvoryaninov, G.S., and A.V. Prusov, 1978: Theoretical model of mass transport by gravity and tidal waves, Oceanology, 18, 640-647.

Fjeldstad, J.E., 1929: Contribution to the dynamics of free progressive tidal waves, Norwegian North Polar Exped. with the Maud, 1918-1925, Scientific Results, vol. 4, 80 pp.

Grant, W.D., and O.S. Madsen, 1979: Combined wave and current interaction with a rough bottom, J. Geophys. Res., 84, 1797-1808.

Isaji, Q., M. Spaulding and M. Reed, 1984: Circulation Dynamics in the Bering Sea. Private communication, Applied Science Associates, Wakefield, RI.

Lavelle, J.W., and H.O. Mofjeld, 1983: Effects of time-varying viscosity on oscillatory turbulent channel flow. J. Geophys. Res., 88, 7607-7616.

Liu, S.-K., and J.J. Leenderste, 1978: Three-dimensional subgridscale-energy model of the eastern Bering Sea. Proc. XVI Coast. Eng. Conf., Amer. Soc. Civil Eng.

Liu, S.-K., and J.J. Leenderste, 1979: A Three-Dimensional Model for Estuaries and Coastal Seas: VI Bristol Bay Simulations. The Rand Corp., R-2405-NOAA.

Liu, S.-K., and J.J. Leenderste, 1982: A three-dimensional shelf model of the Bering and Chukchi Seas, Amer. Soc. Civil Eng., Coastal Engineering, 18, 598-616.

Liu, S.-K., and J.J. Leenderste, 1984: Modeling the Alaska Coastal Waters, in Three-Dimensional Shelf Models (ed. by N. Heaps), Amer. Geophys. Union, Washington, D.C., in press.

Longuet-Higgins, M.S., 1969: On the transport of mass by time-varying currents. Deep-Sea Res., 16, 431-447.

Mellor, G.L., and T. Yamada, 1974: A hierarchy of turbulence closure models for planetary boundary layers. J. Atmos. Sci., 31, 1791-1806.

Mellor, G.L., and T. Yamada, 1982: Development of a turbulence closure model for geophysical fluid problems. Rev. Geophys. Space Phys., 20, 851-875.

Mofjeld, H.O., 1980: Effects of vertical viscosity on Kelvin waves. J. Phys. Oceanogr., 10, 1040-1050.

Mofjeld, H.O., and J.W. Lavelle, 1983: Bottom boundary layer studies in tidally-dominated regimes. XVIII General Assembly of the Union of Geodesy and Geophysics, Hamburg FRG, IUGG-IAPSO Programme and Abstracts.

Mofjeld, H.O., and J.W. Lavelle, 1984: Setting the length scale in a second-order closure model of the unstratified bottom boundary layer. J. Phys. Oceanogr., 14, 832-839.

Mofjeld, H.O., 1984: Recent observations of tides and tidal currents from the Northeastern Bering Sea Shelf, NOAA Technical Memorandum, ERL PMEL-57, 36 pp.

Overland, J.E., H.O. Mofjeld and C.H. Pease, 1984: Wind-driven ice drift in a shallow sea. J. Geophys. Res., 89, 6525-6531.

Pearson, C.A., H.O. Mofjeld and R.B. Tripp, 1981: The tides of the Eastern Bering Sea Shelf. In: The Eastern Bering Sea Shelf: Oceanography and Resources. D.H. Hood and J.A. Calder, Eds., University of Washington Press, 111-130, 625 pp.

Schumacher, J.D., and T.H. Kinder, 1983: Low-frequency current regimes over the Bering Sea Shelf. J. Phys. Oceanogr., 13, 607-623.

Smith, J.D., and C.E. Long, 1976: The effect of turning in the bottom boundary layer on continental shelf sediment transport, Mémoires Société Royale des Science de Liège, 6^{e} séries, tome X, 369-396.

Sündermann, J., 1977: The semidiurnal principal lunar tide M2 in the Bering Sea. Deutsche Hydrog. Zeitschrift, 30, 91-101.

Sverdrup, H.U., 1927: Dynamics of tides on the North Siberian Shelf. Geofis. Publ., 4, 75 pp.

Thorade, H., 1928: Gezeitenumtersuchungen in der Deutschen Bucht der Nordsee, Archiv. Dtsch. Seewarte Hamburg, 46, (see Defant, 1961).